



People's Democratic Republic of Algeria  
Ministry of Higher Education and Scientific Research  
SAAD DAHLEB University Blida 1



**Institute of Aeronautics and Space Studies  
Aeronautical construction department**

*MANUSCRIPT SUBMITTED*

*FOR THE DEGREE OF MASTER IN AERONAUTICS*

*Speciality: Avionics*

***Quadrotors attitude estimation and control  
with Arduino implementation***

Presented by

Khettal Fairouz  
Doumi Nouha Wissem

Supervised by

Mr Choutri  
Mr Lagha

Blida 2020,2021

## **Acknowledgement**

We would like to express our deep gratitude to ALLAH for giving us the strength, patience and willingness to do this work.

We warmly thank all the people who helped us during the development of our master manuscript and in particular our promoter Mr. Choutri Kheireddine and Mr. Professor Lagha Mohand, for their interest and their support, their availability and their many advices during the drafting of this manuscript.

This work would not have been possible without the support of the Institute of Aeronautics and Space Studies BLIDA which allowed us, thanks to a research allowance and various financial aids, to devote ourselves serenely to the development of this manuscript.

This project could not have been carried out without the availability and the warm welcome shown to us by Mr. Safer Salim at ENTA, Mr. Boukettab at the ENTA laboratory, the director of the CRD Mr. Medjahed Rabah and a special thanks to Mr. Benkherouf Toufik and Mr Mehaya Hamza for being close to us each time we needed them and provided us with valuable documents to move forward in this research. The many witnesses we had the opportunity to interview as part of this work notably Mrs Aziza, have enabled us we hope, to bring this story to life.

At the end of this journey, I finally thank those who are dear to us and whom we have somewhat neglected in recent months to complete this manuscript. Their attentions and encouragement have accompanied us throughout these years. We are indebted to our parents for their moral and material support and their unwavering confidence in our choices.

We thank all the jury members for the honor they gave us when accepting to have a look on our job and examine it.

Finally, a special thought to our friends who contributed from near or far to make this memory successful.

## **Dedicate**

We would like to dedicate our dissertation work to our parents, our families and friends who have supported us throughout this critical and special period.

We are really unable to find the right words to tell you thank you for your encouragements. Without your love and help, we wouldn't have reached this success.

We feel very grateful towards our parents, and all words we use to thank them are insufficient. Thank you for being so patient and comprehensive during all these years, without your encouragement and support, we would have been lost. Thank you for all the sacrifices you did for us. Your advices let us become what we are today. We feel very lucky to have you by our side.

We dedicate at the end, this master manuscript, to each person, whose help, advice and assistance, have allowed us to overcome all the obstacles which have stood in our way, or which have been to our sides or heart with us, from the beginning to the end of this journey.

## ملخص:

أحرزت الطائرات بدون طيار تقدماً كبيراً في السنوات الأخيرة. في مخطوطتنا الرئيسية، سوف نركز بشكل خاص على المروحيات الرباعية من حيث إنجازها والتحكم فيها بواسطة لوحة اردوينو دويو.

أولاً، تم تطوير النموذج الديناميكي باستخدام شكلية نيوتن أويلر من أجل التعرف على جميع التأثيرات الجيروسكوبية التي تؤثر على الطائرة الرباعية، شرعنا في تجميع المكونات المختلفة ومعايرتها. بعد ذلك تم استخدام طريقة تحديد الهوية لحساب معالم الطائرة الرباعية، ثم لتحقيق التشغيل المستقل، تم تقدير الحالة باستخدام مستشعرات مختلفة. كما تمت صناعة مقاعد اختبار بهدف تثبيتها.

الاختبارات التي تم إجراؤها قاطعة وذات نتيجة فقد مكنتنا من التحكم في الطائرة الرباعية عن طريق ثلاث وحدات تحكم.

**الكلمات المفتاحية:** الطائرات بدون طيار، النموذج الديناميكي، تقدير الحالة، التحكم في الحالة.

## Abstract

The use of drones or unmanned aerial vehicles UAVs has grown considerably in recent years. In this work we were interested in the realization and state control of a Quadrotor based on an Arduino Due board.

First the dynamic model was developed using Newton-Euler formalism in order to mention all the gyroscopic effects acting on the Quadrotor. We proceeded to assemble the various components and their calibrations. The identification method was used to calculate the parameters of the Quadrotor, then to allow autonomous operation, a state estimate was developed using attitude sensors. A test bench was carried out in order to stabilize this Quadrotor. The tests carried out are conclusive and have enabled us to control the Quadrotor via a PID command.

**Key words:** UAV, Quadrotor, Dynamic Model, State Estimate, State Control, PID command.

## Résumé

L'utilisation des drones ou véhicules aériens sans pilote UAV a considérablement progressé ces dernières années. Dans ce travail on s'est intéressé à la réalisation et le contrôle d'état d'un Quadrirotor à base d'une carte Arduino Due.

D'abord le modèle dynamique a été développé en utilisant le formalisme de Newton-Euler afin de mentionner tous les effets gyroscopiques agissant sur le Quadrirotor. Nous avons procédé à l'assemblage des différents composants et de leurs calibrages. La méthode d'identification a été employée pour calculer les paramètres du Quadrirotor, puis pour permettre le fonctionnement autonome, une estimation d'état a été élaborée à l'aide de capteurs d'attitude. Un banc d'essai a été réalisé dans le but de procéder à la stabilisation de ce Quadrirotor. Les essais effectués sont concluants et nous ont permis de contrôler le Quadrirotor via une commande PID.

**Mots clés :** Véhicules Aériens Sans Pilote, Quadrirotor, Modèle Dynamique, Estimation D'état, Control d'état, Commande PID.

# Content

Acknowledgement.....	I
Dedicate.....	II
Abstract .....	III
List of figures .....	VII
List of tables.....	IX
Acronyms.....	X
List of symbols .....	XI
General Introduction .....	1
<b>Chapter I: Generalities and components</b>	
I.1 Introduction .....	3
I.2 Definition of unmanned aerial vehicles .....	3
I.3 Classification of unmanned aerial vehicles .....	3
I.3.1 According to the size .....	4
I.3.2 According to the propulsion mode.....	4
I.3.3 New drones.....	7
I.4 Quadrotors.....	8
I.4.1 Advantages of Quadrotors.....	9
I.4.2 Disadvantages of Quadrotors .....	9
I.5 Components.....	9
I.5.1 Frame:.....	9
I.5.2 Flight Controller .....	10
I.5.3 Propellers.....	11
I.5.4 Brushless motors .....	11
I.5.5 Electronic Speed Controller .....	13

I.5.6 Battery .....	14
I.5.7 Radio Transceiver .....	15
I.6 Conclusion .....	17

## Chapter II: System modelling

II.1 Introduction .....	19
II.2 The movements of Quadrotor .....	19
II.2.1 Vertical movement .....	19
II.2.2 Roll movement.....	19
II.2.3 Pitch movement.....	19
II.2.4 Yaw movement.....	20
II.2.5 Translational movements .....	20
II.3 Dynamic modelling.....	22
II.3.1 Rotation matrix.....	22
II.3.2 Angular velocity .....	23
II.3.3 Linear velocity.....	24
II.3.5 Development of the mathematical model .....	26
II.3.6 Rotor dynamics.....	29
II.4 Conclusion.....	33

## Chapter III: Quadrotor Identification and Control

III.1 Introduction .....	36
III.2 Parameters Identification .....	36
III.2.1 Total mass.....	36
III.2.2 Inertia matrix "I" .....	37
III.2.3 Lift coefficient "b" .....	43
III.2.4 drag coefficient "d" .....	44
III.3 State estimation .....	45
III.4 Control system architecture design .....	49

III.4.1 Quadrotor modelling for control .....	49
III.4.2 Brushless motor block .....	50
III.4.3 PID controller block .....	52
III.5 Simulation .....	52
III.6 Conclusion .....	54

## Chapter IV: Hardware Implementation

IV.1 Introduction .....	56
IV.2 System architecture .....	56
IV.2.1 Sensors .....	57
IV.2.2 Emission part .....	60
IV.2.3 Reception part .....	62
IV.3 Quadrotor Assembly .....	65
IV.4 Calibrations .....	66
IV.5 Test Bench .....	67
IV.6 PID Tuning and Regulation .....	69
IV.7 Conclusion .....	69
General Conclusion .....	70
Appendix .....	72
Bibliography .....	77

# List of figures

## Chapter I

<i>Figure(I-1): Fixed wing drone</i> .....	5
<i>Figure (I-2) : Flapping wing drone</i> .....	5
<i>Figure (I-3): Mono rotor drone</i> .....	5
<i>Figure (I-4): Coaxial drone</i> .....	6
<i>Figure (I- 5): Quadrotor drone</i> .....	6
<i>Figure (I-6): Multi rotor drone</i> .....	6
<i>Figure (I-7): Wing long II drone</i> .....	7
<i>Figure (I-8): DJI Air 2S drone</i> .....	7
<i>Figure (I-9): FLIRTEY drone</i> .....	8
<i>Figure (I-10): EHANG drone</i> .....	8
<i>Figure (I-11): Frame F-450</i> .....	10
<i>Figure (I-12) : Up, Arduino Due board (top side). Down, Arduino Due board (bottom side)</i> .....	10
<i>Figure (I-13): 8045 propellers</i> .....	11
<i>Figure (I-14) : 1000KV Brushless Motor</i> .....	13
<i>Figure (I-15): Electronic speed controller 40A</i> .....	13
<i>Figure (I-16) : LI-PO 4S 3000mah 20-30c battery</i> .....	14
<i>Figure (I-17) : Battery discharge graphic curve</i> .....	15
<i>Figure (I-18) : RF24 module.</i> .....	16

## Chapter II

<i>Figure (II -1): vertical motion in cross quadrotor</i> .....	21
<i>Figure (II -2): Right roll motion in cross quadrotor</i> .....	21
<i>Figure (II -3): Forward pitch motion in cross quadrotor</i> .....	21
<i>Figure (II -4) : Yaw Counterclockwise motion in cross quadrotor</i> .....	21
<i>Figure (II -5) : Body coordinate system</i> .....	23
<i>Figure (II-6): brushless DC motor schematic at steady state</i> .....	30
<i>Figure (II -7): Star assembly of BLDC motor</i> .....	32

## Chapter III

<i>Figure (III -1) : balance for measuring quadrotor mass</i> .....	37
<i>Figure (III -2) : The bifilar pendulum experiment</i> .....	37
<i>Figure (III -3): cross structure identification</i> .....	38
<i>Figure (III -4): The rectangular parallelepiped identification</i> .....	39
<i>Figure (III -5) : The motors identification</i> .....	40
<i>Figure (III -6): Propellers identification</i> .....	41
<i>Figure (III -7): Motor gear identification.</i> .....	42
<i>Figure (III -8): Motor propeller motor gear assembly identification.</i> .....	43
<i>Figure (III -9) : MPU operating diagram</i> .....	46
<i>Figure (III -10): Overview of Madgwick Filter</i> .....	47



<b>Figure (III -11): control system architecture .....</b>	<b>49</b>
<b>Figure (III -12): Battery discharge algorithm structure .....</b>	<b>51</b>
<b>Figure (III -13): The measured attitude compared to attitude desired (<math>K_p=3</math>, <math>k_d=0.8</math>, <math>k_i=0.08</math> for Roll and Pitch. <math>K_p=2.8</math>, <math>k_d=0.4</math>, <math>k_i=0.03</math> for Yaw angle).....</b>	<b>53</b>
<b>Figure (III -14): Simulation results with desired angles roll =1, pitch=1, yaw=1.....</b>	<b>53</b>

## *Chapter IV*

<b>Figure (IV-1): Realization architecture.....</b>	<b>56</b>
<b>Figure (IV -2) : MPU 9250 motions along the three axis .....</b>	<b>57</b>
<b>Figure (IV -3): MPU 9250 sensor .....</b>	<b>58</b>
<b>Figure (IV -4): HC-S04 SONAR sensor.....</b>	<b>58</b>
<b>Figure (IV -5) : Infra-Red Sensor.....</b>	<b>59</b>
<b>Figure (IV-6): GPS neo-7m module .....</b>	<b>60</b>
<b>Figure (IV -7): Emission circuit .....</b>	<b>61</b>
<b>Figure (IV -8) : Assembly of the transmission circuit .....</b>	<b>62</b>
<b>Figure (IV -9): GPS module Wiring .....</b>	<b>63</b>
<b>Figure (IV -10): MPU9250 module wiring .....</b>	<b>63</b>
<b>Figure ( IV -11): Sonar Module Wiring. ....</b>	<b>64</b>
<b>Figure (IV -12): IR module wiring.....</b>	<b>64</b>
<b>Figure (IV-13): RF24 module Wiring .....</b>	<b>64</b>
<b>Figure (IV -14): The general circuit of the quadrotor.....</b>	<b>65</b>
<b>Figure (IV -15): Quadrotor assembly .....</b>	<b>65</b>
<b>Figure (IV -16): Quadrotor and PCB assembly.....</b>	<b>66</b>
<b>Figure (IV -17): Single axis test bench.....</b>	<b>67</b>
<b>Figure (IV -18): Back view of the three frames test bench.....</b>	<b>68</b>
<b>Figure (IV -19) : Two wires test bench.....</b>	<b>68</b>

## *Appendix*

<b>Figure (A-1): Simulink model of the quadrotor.....</b>	<b>72</b>
<b>Figure (A -2) : PID controller Simulink Block. ....</b>	<b>73</b>
<b>Figure (A -3): Brushless motor Simulink block. ....</b>	<b>73</b>
<b>Figure (A -4): TF BLDC.....</b>	<b>73</b>
<b>Figure (A -5) : Quadrotor model Simulink block. ....</b>	<b>74</b>
<b>Figure (A-6): U Calculator .....</b>	<b>74</b>
<b>Figure (A -7): Angles.....</b>	<b>61</b>
<b>Figure (A -8) : XYZ Position .....</b>	<b>75</b>

# List of tables

## *Chapter I*

<b>Table (I-1) :</b> <i>A2212-1000KV Brushless Motor specifications</i> .....	12
<b>Table (I-2) :</b> <i>ESC 40A specifications</i> .....	14
<b>Table (I-3) :</b> <i>Li-Po battery characteristics</i> .....	15

## *Chapter II*

<b>Table (II -1) :</b> <i>1000kv BLDC parameters</i> .....	33
--	----

## *Chapter III*

<b>Table (III -1) :</b> <i>Quadrotor parameters obtained by identification</i> .....	44
--	----

## *Chapter IV*

<b>Table (IV -1):</b> <i>MPU 9250 specifications</i> .....	57
<b>Table (IV -2) :</b> <i>InfraRed specifications</i> .....	59
<b>Table (IV -3):</b> <i>GPS neo-7m-0-000 technical specifications</i> .....	60
<b>Table (IV-4):</b> <i>The pinout specifications of the emission circuit</i> .....	60
<b>Table (IV -5) :</b> <i>The pinout specifications of the reception circuit</i> .....	63
<b>Table (IV -6) :</b> <i>PID gains representation</i> .....	69

# Acronyms

<b>BLDC</b>	Brush Less Direct Current Motors.
<b>DoF</b>	Degrees-of-Freedom .
<b>ESC</b>	Electronic Speed Controller.
<b>GPS</b>	Global Positioning System.
<b>HALE</b>	High Altitude Long Endurance.
<b>IMU</b>	Inertial Measurement Unit.
<b>IR</b>	Infra Red.
<b>LIPO</b>	Lithium-POLymer.
<b>MALE</b>	Medium Altitude Long Endurance.
<b>PCB</b>	Printed Circuit Board.
<b>PID</b>	Proportional Integrator Derivative.
<b>PWM</b>	Pulse Width Modulated.
<b>RPM</b>	Revolution Per Minute.
<b>SONAR</b>	SOund Navigation And Ranging.
<b>UAV</b>	Unmanned Aerial Vehicle.
<b>VTOL</b>	Vertical Take-Off and Landing.

## List of symbols

$\varphi$	roll angle.
$\theta$	pitch angle.
$\psi$	yaw angle.
$OE, xE, yE, zE$	earth frame coordinates
$OB, xB, yB, zB$	body frame coordinates
$R$	rotation matrix
$\Omega$	angular velocity in the fixed frame
$V$	body linear speed
$P$	body weight
$m$	overall mass
$g$	Gravity
$F_i$	thrust force
$b$	thrust coefficient
$T_h$	drag in the propellers
$d$	drag coefficient
$K_{ft}$	the translational drag coefficient
$M_x, M_y, M_z$	moment around the (x, y, z) axes
$l$	horizontal distance: propeller center to center of gravity of Quadrotor
$M_a$	moment resulting from aerodynamic friction.
$K_{fa}$	the coefficient of aerodynamic friction.
$M_{gh}$	gyroscopic moment of the propellers .
$J_r$	Rotors inertia.
$M$	gyroscopic moment due to quadrotor movements.
$J$	system inertia.
$\zeta$	position vector of the quadrotor.
$S(\Omega)$	anti symmetric matrix.
$F_f$	total force generated by the four rotors
$F_t$	drag force along the (x, y, and z) axes
$F_g$	force of gravity.
$M_f$	moment caused by push and drag forces
$\Omega_r$	the overall propellers speed
$V_s$	DC source voltage
$i$	armature current
$T_e$	electrical Torque.
$K_f$	friction constant .
$\omega_m$	angular velocity.
$T_L$	supposed mechanical load.
$K_e$	back emf constant.
$K_t$	torque constant.
$G(s)$	BLDC transfer function.
$\tau_m$	mechanical time constant.

$\tau_e$	electrical time constant.
$T$	oscillation period of a cycle (s).
$r$	radius between the points of the two chords (m).
$L$	length of the two chords.
$I_C$	cross structure moment of inertia.
$I_e$	electronics box moment of inertia.
$I_{MIX}$	motor moment of inertia.
$I_{MGIX}$	motor gear moment of inertia.
$I_{PIX}$	propeller gear moment of inertia.
$I_{XX,YY,ZZ}$	inertia moments.
$\alpha$	the angle of incidence of the propeller.
$D_E$	electronics box to COM distance around the z-axis.
$D_M$	motor to COM distance around the z-axis.
$D_{MG}$	motor gear to COM distance around the z-axis.
$D_P$	propeller to COM distance around the z-axis.
$H_E$	electronics box height.
$H_M$	motor height.
$H_{MG}$	motor gear height.
$H_P$	propeller height.
$L_C$	cross structure length.
$L_E$	electronics box length.
$L_M$	motor to COM distance around the x-axis.
$L_{MG}$	motor gear to COM distance around the x-axis.
$L_P$	propeller to COM distance around the x-axis.
$M_C$	half cross structure mass.
$M_E$	electronics box mass.
$M_M$	motor mass.
$M_{MG}$	motor gear mass.
$M_P$	propeller mass.
$R_C$	cross structure radius.
$R_M$	motor radius.
$R_{MG}$	motor gear radius.
$R_P$	propeller radius.
$W_E$	electronics box width.
$U$	generic controlled variable.
$e$	the error between the task $r$ and the process output $y$ .
$K_p$	the proportional gain
$K_i$	the integral gain
$K_d$	the derivative gain
$\varphi_d$	the desired roll angle.
$\varphi$	the measured roll angle.
$e_\varphi$	the roll error .
$U_2$	the required roll torque.

$\theta_d$	the desired pitch angle.
$\theta$	the measured pitch angle.
$e_\theta$	the pitch error .
$U_3$	the required pitch torque.
$\psi_d$	the desired yaw angle.
$\psi$	the measured yaw angle.
$e_\psi$	the yaw error.
$U_4$	the required yaw torque.
$C$	constant discharge.
$B$	inverse gyroscope weight
$W_{\hat{g}}$	the normalized gravity vector
$I_{\hat{a}}$	the normalized acceleration
$\hat{x}$	normalized x.
$I_{\omega_t}$	gyro measurements
$I_{\hat{a}_t}$	accelerometer measurements

## General Introduction

For the past ten years, technical advancements have permitted the design and building of mini-planes or helicopters with ever-increasing capacity to undertake autonomous flights, allowing humans to be replaced by autonomous robots in more efficient and safer ways such as firefighting. These devices are known as UAVs.

In this field, research or concept development is mostly multidisciplinary. Indeed, the design of an unmanned aerial vehicle (UAV) necessitates a variety of fields, including electronics, automatics, informatics, mechanics, robotics, communication and especially aeronautics.

The quadrotor cross architecture has been chosen for this research for its low dimension, good maneuverability, simple mechanics and payload capability.

In addition to this final-year-of-study-thesis, the work that will be done aim to answer some questions like: what are the electronic, electrical, mechanical, automatic, aerodynamic, avionic, or robotic characteristics of a quadrotor style UAV and how do we design an embedded control system for an unmanned aerial vehicle.

The objectives of this thesis are to model the system, state estimate and control, construct a simulator, and develop a real platform, as well as to observe drone behavior. This master manuscript is structured as follows:

The first chapter, gives a definition of the UAVs, then the main types of drones and their classification according to their size and their applications were introduced. In the second part, we defined the quadrotor and its usefulness. We have briefly presented some new drones. Then we mentioned the components used to realize this project.

The second chapter, provides the modelling of a quadrotor, we have seen the different movements of a quadrotor .This chapter deals with the aerodynamics of the quadrotor using the formalism of Newton-Euler. A quadrotor may be thought of as a rigid body with six degrees of freedom. First, we have presented the benchmarks necessary to express orientation of the quadrotor. Second, we identified all the forces, moments and effects impacting the quadrotor. Finally, we presented the rotor dynamics and its transfer function.

The third chapter was devoted to estimate and control the state, the calculation of parameters of the quadrotor was necessary to identify our model and to simulate it thereafter. The simulation was done in order to estimate the system response and compare it with the realization results as well to approximate the ideal PID gains corresponding to our system.

And finally, the fourth chapter shows the developing process of the quadrotor platform. To give a visual description, a few photos have been added. Then, we carried out the quadrotor assembly while respecting the conventions in the connections. Once the final assembly was done, it was necessary to configure and calibrate the flight controller based on an Arduino Due board, and adjust the parameters of the control to ensure the stability of the quadrotor using several test benches. Finally, the experimental results of the stabilization algorithm are reported.

# **Chapter I:**

## **Generalities and components**



## **I.1 Introduction**

Lately the development and investigation of autonomous flight systems have increased because of the increasing amount of applications of unmanned aerial vehicle (UAV) in military fields such as intelligence, surveillance, and reconnaissance missions, and in civil fields like aerial surveillance, aerial photography and video, firefighting, and many missions. In all cases the need to substitute human intervention in high-risk tasks is the impetus for research in this field. Indeed it involves very varied fields such as aerodynamics, signal and image processing, automatic control, mechanics, composite materials, real-time computing, Etc.

In this master manuscript, we are particularly interested in air vehicles miniatures and more particularly to a Quadrotor.

Quadrotor drones are among the most complex of flying objects, because their flight dynamics is inherently nonlinear, and the variables are strongly coupled.

## **I.2 Definition of unmanned aerial vehicles**

The definition of UAVs varies from one literature to the other. For our purposes, UAVs are small aircrafts, capable of carrying out missions more or less autonomously. [1]

The main function of these aerial vehicles is to extend human vision beyond the natural horizon, in order to perform work at risk or in hostile environments. They have played a key role in carrying out reconnaissance, information gathering and even combat operations.

Autonomous vehicles are controlled by an onboard computer that can be preprogrammed to perform a specific task or a broad set of tasks. While in other literatures, UAVs may refer to powered or unpowered, tethered or untethered aerial vehicles.

## **I.3 Classification of unmanned aerial vehicles**

Here are different ways to classify UAV's, either according to their size or according to their propulsion mode.

## I.3.1 According to the size

**HALE** (High Altitude Long Endurance): These are large drones, most often fixed-wing. They are able to stay in flight for a very long time and collect information's on very long periods (between 12 and 48 hours). They can fly over 15000 meters high.

**MALE** (Medium Altitude Long Endurance): These are used for long duration flights at medium altitude operational between 5000- 15000 meters for a maximum of 24hours, with great autonomy. They have a relatively high payload of 10 kg enabling having heavy and high quality navigation sensors on board.

Both of these two types of drones are part of the large size class. They can carrying weapons, which usually requires having a human in the loop, which last must keep the decision to fire and be able to cancel the mission at any time.

**Mini drones:** They are able to fly indoor and outdoor flight. These are light drones and small in size (a payload of less than 2 kg which is sufficient to carry small lightweight with sensors and a wingspan of up to 1 to 2 meters), they have an autonomy relatively low (10 to 30 minutes) and generally used for observation of hard-to-reach areas.

**Micro drones:** These are drones with sizes varying from centimeter to a few tens of centimeters. They have a payload of less than 100 grams. Usually electrically powered. They allow for indoor flights. They carry small loads.

## I.3.2 According to the propulsion mode

We can also classify drones according to the aerodynamic functioning of which we find:

**Fixed-wing drones:** Are drones that travel with fixed wings. They are primarily employed for scientific purposes including meteorically reconnaissance and environmental monitoring.



*Figure (I-1): Fixed wing drone*

**Flapping wing drones:** bird or insect type. These UAVs have small wings and have an extremely low payload and endurance.

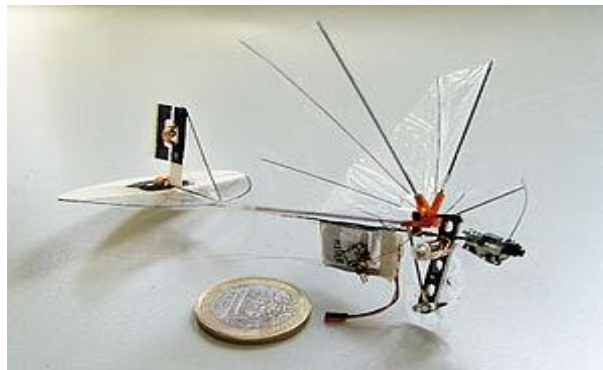


*Figure (I-2): Flapping wing drone*

**Rotary wing drones:** This type of drones are subdivided into several subclasses in which we find:

*Mono-rotor:* They have a main rotor on top and another rotor at the tail for stability, same like the helicopter configuration.



*Figure (I-3): Mono rotor drone*

*Coaxial:* They have two rotors rotating in opposite directions mounted to the same shaft.



**Figure (I-4):** *Coaxial drone*

*Quadrotor:* UAVs composed of four rotors



**Figure (I- 5):** *Quadrotor drone*

*Multi-rotor:* UAVs with six or eight rotors.



**Figure (I-6):** *Multi rotor drone*

This thesis work focuses on the study of a Vertical Take-Off and Landing (VTOL) Unmanned Aerial Vehicle (UAV). The proposed structure is a four propeller helicopter called Quadrotor.

## I.3.3 New drones

The age of drones has arrived, self-driving and self-flying vehicles are becoming more of a reality. Companies ranging from start-ups to major corporations such as Google and Amazon are vying for a piece of the sky, examining the best ways to incorporate drones into our daily lives, in the following section we present some examples of new drones.

- **Wing long II**

China Deploys Drone to Restore Communications During Flood Disaster WING LONG II. The drones have a range of up to 35 hours of communication time. So they can be used to restore communications by acting as a bridge between mobile phones and satellites without base station coverage. While satellite communication is slower, it is not impacted by weather on the ground.



*Figure (I-7):* Wing long II drone

- **DJI Air 2S**

The best drones for shooting stunning aerial photos and video. It has the ability to perceive its environment in four directions: up, down, forward, and backward. The Max Hovering Time (at no wind) is 30 minutes and a camera with effective Pixels: 20MP; 2.4um Pixel Size.



*Figure (I-8):* DJI Air 2S drone

- **FLIRTEY**

Drone deliveries of first aid kits and emergency medication are getting one step closer as Nevada based start-up. FLIRTEY made its own autonomous delivery of food, water and a first aid kit.



*Figure (I-9): FLIRTEY drone*

- **EHANG**

EHang has signed a contract with Lung Biotechnology PBC in US to develop up to 1,000 units of its 184 drones, the world's first autonomous drone capable of transporting a human. The purpose is to automate transportation of donated organs to people all over the country in emergency situations. [2]



*Figure (I-10): EHANG drone*

## **I.4 Quadrotors**

A quadrotor has four rotors, each one of which has independent speed, allowing a balanced variation of the rotor's speed and thus generating the thrust and accelerations in the desired directions. Quadrotors are six-degrees-of-freedom (DOF) systems, what means that

they can move along the three space axes X, Y and Z, and turn on the aircraft's body axes describing roll ( $\phi$ ), pitch ( $\theta$ ) and yaw ( $\psi$ ) angles. [3]

## I.4.1 Advantages of Quadrotors

Quadrotors have many advantages, among these advantages:

- Precise and Handy.
- Allows the maintenance of a GPS position and an altitude.
- Economic > 10 times less expensive than traditional solutions.
- Very portable and easy to store.
- Less complicated than other multi-rotors which have multiple engines.
- Excellent flight time.
- Limit and avoid human risks in hazardous environments.
- Can perform highly flexible missions.

## I.4.2 Disadvantages of Quadrotors

The disadvantages of quadrotors are as follows:

- No motor redundancy. When one of the motors fails, the drone cannot continue to fly.
- Less precise and less stable compared to the Hexarotor.
- Very unstable in turbulent flight conditions.
- Less thrust than the Hexarotor.
- There are very few elements available in terms of reliability study, maintenance concept on drones in general and acquisition and support costs in particular.

## I.5 Components

Here we will enlist the components required in this project

### I.5.1 Frame:

Because the frame is sensitive to vibrations caused by motors and propellers, we chose an "X" shaped F450 (Wingspan: 450mm) made of high-quality glass fiber and polyamide nylon, which is lighter and more stable than some other materials. The F450 frame includes integrated PCB connectors for direct ESC soldering, making esc, power supply, and other cabling more efficient and durable. (See Figure I.11)





**Figure (I-11):** *Frame F-450*

## I.5.2 Flight Controller

The flight controller used in our project is based on an Arduino board, precisely we use the Arduino Due board which is a microcontroller board based on the Atmel SAM3X8E ARM Cortex-M3 CPU. It is the first Arduino board based on a 32-bit ARM core microcontroller. It has 54 digital input/output pins (of which 12 can be used as PWM outputs), 12 analog inputs, 4 UARTs (hardware serial ports), a 84 MHz clock, an USB OTG capable connection, 2 DAC (digital to analog), 2 TWI, a power jack, an SPI header, a JTAG header, a reset button and an erase button with 3.3V operating voltage. [4]

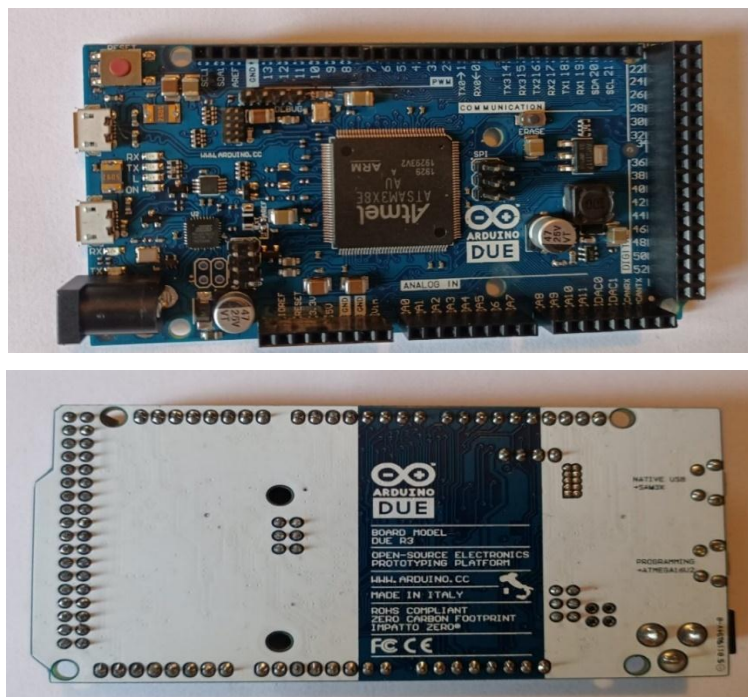


**Figure (I-12):** *Up, Arduino Due board (top side). Down, Arduino Due board (bottom side)*



## I.5.3 Propellers

The propellers are at the heart of the drone's propulsion. We used 4 blades directly attached to motors two of them are rotating clockwise and two others rotate anticlockwise (a pusher and a puller).

For better performance and less battery consumption, we have chosen the 8045 presented in the figure (I.13) below which simply means a length of 8 inches and a pitch of 4.5 inches made with high quality ABS Plastic for maximum performance, rigidity, durability and balance.

A short propeller will spin faster than a long propeller because the aerodynamic surface is smaller. It will have less lift but will provide responsiveness in flight.

The pitch of a propeller defines the distance it travels when it makes a full turn. High pitch implies low lift but high maximum rotational speed. A smaller pitch implies a better lift but a limited maximum rotation speed. The pitch is adapted by the manufacturer.

To know in which direction the propellers must turn, it suffices to define the leading edge and the trailing edge of a propeller so we have to choose the direction where the air crosses the leading edge and escapes through the trailing edge. The propeller reference is always in the top.

Simpler, the direction of opening of the propeller is the same direction of rotation of the motor, it is the same principle as a screw and nut.

In our first experiment we noticed that the air escapes above so we reversed the propellers so that the air escapes below to be able to raise the drone.



**Figure (I-13):** 8045 propellers

**Remark:** For acrobatic flight, we prefer short propellers providing responsiveness to the drone. For stable flight, we prefer long propellers providing stability.

### I.5.4 Brushless motors

The type of motors depends on the choice of propellers. It is necessary to define for what kind of application is intended the drone which will support these engines and the final weight of the device. These motors are identical to traditional DC motors, however; they do not have any brushes. [5]

Brushless motors were chosen for our project because they have several advantages over brushed DC motors, including a higher torque-to-weight ratio, increased efficiency (producing more torque per watt), increased reliability, reduced noise, longer lifetime (due to the elimination of brush and commutator erosion), elimination of ionizing sparks from the commutator, and a reduction in overall electromagnetic interference. The motor that we have used is A2212 1000KV Brushless Motor with the following characteristics:

**Table (I-1) :** *A2212-1000KV Brushless Motor specifications*

No of cells	2-3 Li-Poly 6-10 NiCd/NiMH
Kv	1000 RPM/V
Max Efficiency	80 %
Max Efficiency Current	4-10A (>75%)
No Load Current	0.5A 10V
Resistance	0.090 ohms
Max Current	13A for 60S
Max Watts	150W
Weight	52.7 g/1/86 oz
Size	28 mm dia x28 mm bell length

The two parameters that must be taken into consideration are: the maximum current consumption, and the number of KV which refers to the constant velocity of a motor, it is measured by the number of revolutions per minute (RPM) that a motor runs when 1V is applied with no load attached to that motor.

In Our case:

$$\begin{cases} KV = 1000 \\ \text{Battery voltage} = 14.8V \end{cases}$$

$$RPM = Motor Kv \text{ racing} \times Battery \text{ voltage} \quad (1.1)$$

$$RPM = 1000 \times 14.8 = 148000 \text{ RPM} \quad (1.2)$$

Two opposite motors must turn clockwise and the other two must turn counter clockwise, because there wouldn't be yaw torque on the system with all motors spinning at the same speed. Now if we want to reverse the direction of rotation of the motor, just switch between two wires which are connected to ESC, this is what we call polarisation.



**Figure (I-14):** 1000KV Brushless Motor

## I.5.5 Electronic Speed Controller

The choice of the electronic speed controller depends on the choice of actuators.

An ESC controls the brushless motor movement or speed by activating the appropriate MOSFETs to create the rotating magnetic field so that the motor rotates. The higher the frequency or the quicker the ESC goes through the 6 intervals, the higher the speed of the motor will be. [6]

On the same side as this connector, there are two thicker wires, one red and one black for the power supply to be connected directly to the general power supply of the drone.



**Figure (I-15):** Electronic speed controller 40A

There are ESCs with BEC (Battery Eliminator Circuit) which embeds a voltage regulator internally and which can be used to power our ARDUINO board, just link the red wire of an ESC\_BEC with the  $V_{in}$  of our ARDUINO board. We used 40A ESC with the following specifications:

**Table (I-2):** ESC 40A specifications

Continuous Output	40A
Bursts Output	60A for 15 seconds
UBEC	5V/3A
Li-Po Battery	2 - 4s (cells)
NiCd/NiMH	5 - 12 cells
Voltage Input	6.4v - 16.8v
Size	71mm x 35mm x 10.5mm
Weight	48g
Motor Type	Brushless Motor
Max RPM	240,000 rpm for a 2 pole, 80,000 rpm for a 6 pole, or 40,000 rpm for a 12 pole brushless motor

## I.5.6 Battery

A lithium-polymer battery is a type of rechargeable battery that uses a soft polymer casing so that the lithium-ion battery inside, it rests in a soft external “pouch.” It may also refer to a lithium-ion battery that uses a gelled polymer as an electrolyte. [7]

LIPO are lighter, high discharging current and capacity, low internal resistance ,long working time and more flexible than other kinds of lithium-ion batteries because of their soft shells, allowing them to be used in mobile and other electronic devices, as well as in our quadrotor’s project.



**Figure (I-16):** LI-PO 4S 3000mah 20-30c battery.

Regarding a Li-Po type battery, each cell has a nominal voltage of 3.7 volts. The elements are connected in series. Their values add up and it will equal 4.2 volts when charged. The number of cells depends on the motor. We select Lithium Polymer (Li-Po) to achieve these characteristics:

**Table (I-3): Li-Po battery characteristics**

Minimum Capacity	3000mAh
Configuration	4S1P / 14.8v / 4Cell
Constant Discharge	20C
Peak Discharge (10sec)	30C
Pack Weight	337g
Pack Size	138 x 44 x 27mm
Charge Plug	JST-XH
Discharge Plug	XT-60

❖ The number of C (constant discharge)

Is the multiplication coefficient of the amperage that the battery can restore during discharge; for example, a 3000mah 30C battery can theoretically supply  $3 \times 30 = 90$  amps. This number enables us to select a battery capable of delivering the current required by our drone.

The number 1 cause of Li-Po degradation is misuse when discharging and each cell should not go below 3, 3 volts according to the figure bellow. [8]

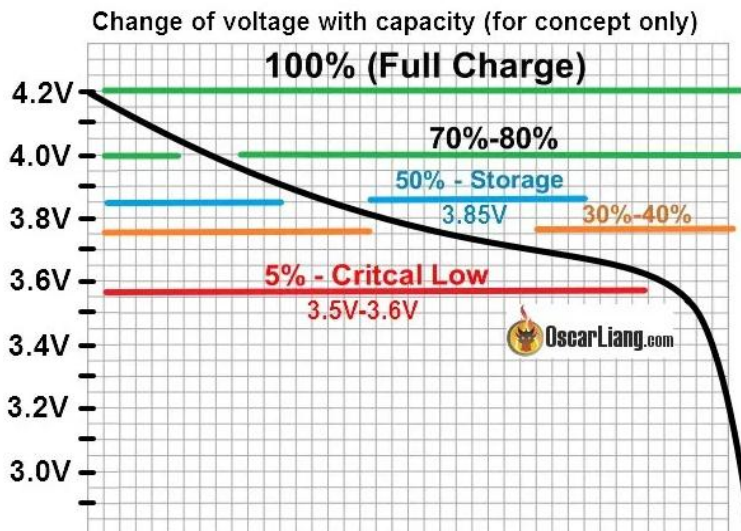


**Figure (I-17): Battery discharge graphic curve**

## I.5.7 Radio Transceiver

We chose HW-237 2.4G 1100 Meters Long-Distance wireless modules NRF24L01+PA+LNA WIFI module with antenna presented in figure (I.18).

NRF24L01 is a single chip radio transceiver for the worldwide 2.4 - 2.5 GHz ISM band. The transceiver consists of a fully integrated frequency synthesizer, a power amplifier, a crystal oscillator, a demodulator, modulator and Enhanced Shock Burst™ protocol engine. Output power, frequency channels, and protocol setup are easily programmable through a SPI interface. Current consumption is very low, only 9.0mA at an output power of -6dBm and 12.3mA in RX mode. Built-in Power Down and Standby modes makes power saving easily realizable. [9]



**Figure (I-18):** RF24 module.

Our Radio transceiver uses SPI communication. The serial peripheral interface (SPI) is a four-wire full-duplex communication protocol that uses MOSI wires (master out slave in), MISO (master in slave out), SCL (a serial clock generated by the master), and SS slave select line (used to pick a specific slave during communication). SPI is a synchronous communication protocol that only supports multi-slave communication and does not support multiple masters.

The SPI has many advantages comparing to I2C communication for example:

- Higher data transfer rate than I2C where SPI can support up to 10MB/s however I2C in the ultra-fast mode can support only 5MB/s
- Maximum Range
- Maximum distance at 1Mbps : 750 meters.

## I.6 Conclusion

In this chapter, we have presented a wide variety of drone families, each of which has its own technical specifications.

The use of drones is developing rapidly in all military fields, and their multiple civilian applications will no doubt spread rapidly once these devices have reached technological maturity, and reducing their cost.

The choice of a drone architecture and material must correspond in particular to the missions for which he will be employed, as well as to the degrees performance wanted.

In the following chapter, we will detail its dynamic model in order to best simulate its behavior.

# **Chapter II:**

# **System modelling**



## **II.1 Introduction**

A Quadrotor is an under actuated aircraft which means number of inputs is less than number of outputs with fixed pitch angle four rotors .

Modeling a vehicle such as a Quadrotor is not an easy task because of its complex structure given the number of physical effects that affect its dynamics namely aerodynamic effects, gravity, gyroscopic effects, friction and moment of inertia. This complexity results essentially from the fact that the expression of these effects differs for each flight mode. The aim is to develop a model of our UAV as realistically as possible.

## **II.2 The movements of Quadrotor**

The basic Quadrotor movements are achieved by varying the speed of each rotor by changing the thrust produced. The Quadrotor tilts towards the direction of the slower rotor, which then allows for translation along that axis. The Quadrotor has five main movements:

### **II.2.1 Vertical movement**

To hover, the entire lift force must be applied along the Z axis and must be equal to or greater than the force of gravity. [10]

The upward and downward movement is achieved by adjusting the motor's rotational speed; if the lift force is higher than the quad-weight, rotor's the movement is upward; if the lift force is less than the quad-weight, rotor's movement is downward. (See Figure II.1)

### **II.2.2 Roll movement**

In this case, we apply a torque around the x axis, i.e. by applying a difference in thrust between the rotors (2&3) and rotors (4&1). This movement (rotation around the x-axis) is coupled with a movement of translation along the y axis [10].

This command is provided by increasing (or decreasing) the propellers (1&4) speed and by decreasing (or increasing) the propellers (2&3). It leads to a torque with respect to the x axis which makes the quadrotor turn. (See Figure II.2)

### **II.2.3 Pitch movement**

In this case, we apply a torque around the y-axis, i.e. by applying a difference in thrust between the rotors (1&2) and rotors (3&4). This movement (rotation around y) is coupled with a movement of translation along the x axis [10].

This command is very similar to the roll and is provided by increasing (or decreasing) the propellers (1&2) speed and by decreasing (or increasing) the propellers (3&4). It leads to a torque with respect to the y axis which makes the quadrotor turn. (See Figure II.3)

### II.2.4 Yaw movement

In this case, we want to apply a torque around the z axis, which is done by applying a speed difference between the rotors (1&3) and (2&4).

This movement is not a direct result of the thrust produced by the motors but by the reactive torques produced by the rotation of the rotors. [10] (See Figure II.4)

### II.2.5 Translational movements

In this case, we want to apply a force along x or y axis which is done by tilting the body (pitching or rolling) and increasing all the motors speed produced to keep the importance of the Z component of the thrust equal to the force of gravity.

On a quadrotor there are two common ways to fly the first is Plus “+” configuration in which a single rotor leads the aircraft, the plus configuration introduces a yaw moment when a pitch or roll control input is introduced; but for the cross configuration, the pitch and roll control is decoupled from the yaw so the four rotors leads the aircraft.

In this project, we chose the cross configuration because it provides more stability than plus configuration.

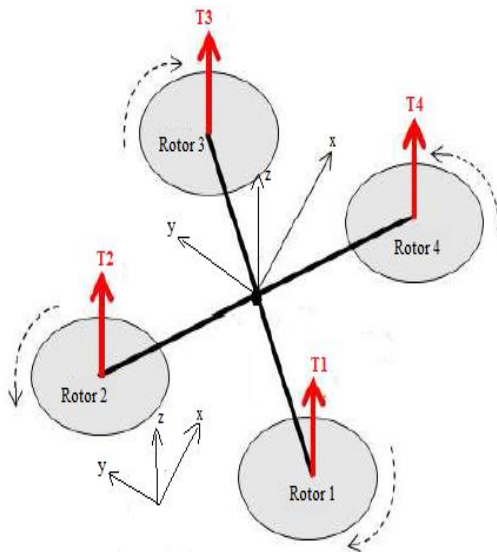


Figure (II -1): vertical motion in cross quadrotor

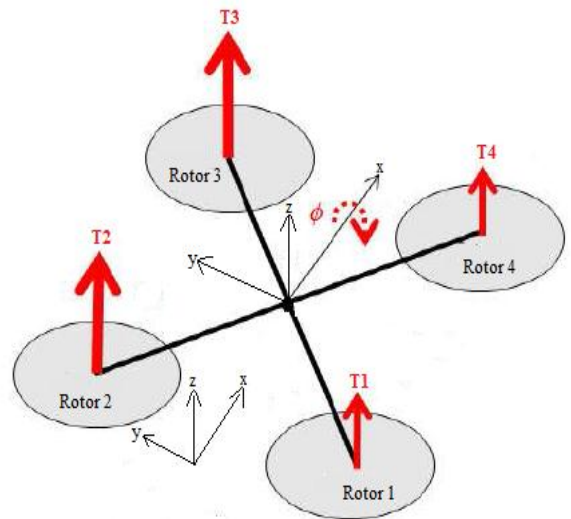


Figure (II -2): Right roll motion in cross quadrotor

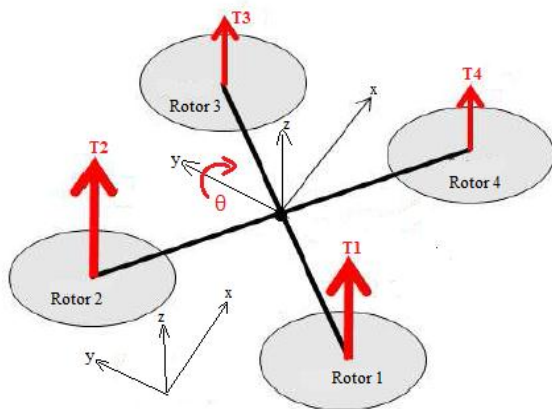


Figure (II -3): Forward pitch motion in cross quadrotor

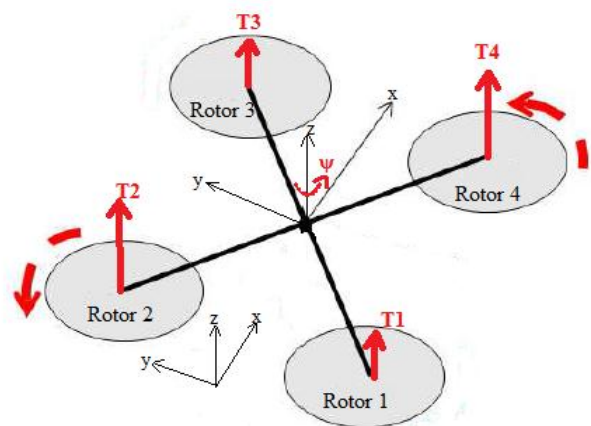


Figure (II -4) : Yaw Counterclockwise motion in cross quadrotor

### II.3 Dynamic modelling

The UAV's modeling is a delicate mission since the dynamics of the system are strongly nonlinear and fully coupled. In order to be able to better understand the dynamic model, we make some assumptions:

- The structure of the Quadrotor is assumed to be rigid and symmetrical, which implies that the matrix of inertia will be assumed to be diagonal.
- The propellers are supposed to be rigid in order to be able to neglect the effect of their deformation during of rotation.
- The center of mass and the origin of the coordinate system related to the structure coincide.
- The lift and drag forces are proportional to the squares of the rotation of rotors.

#### II.3.1 Rotation matrix

To describe the position and orientation of the Quadrotor, we need two frames:

- The first is called the inertial fixed frame  $F_E$  (earth reference frame). It is linked to a point  $O_E$  located on the surface of the earth supposed to be Galilean. The fundamental theorem of mechanics therefore applies to it. We associate with  $E$  the system of axes  $(O_E, x_E, y_E, z_E)$ .
- The definition of a second frame is necessary to describe the orientation of the Quadrotor. This is attached to the frame of the Quadrotor and therefore moves with it. It is called body frame  $F_B$  linked to the  $O_B$  center of gravity. We associates with  $B$  the system of axes  $(O_B, x_B, y_B, z_B)$ .

At the beginning, the body frame coincides with the fixed frame, then the body frame makes a rotational movement around the  $x$  axis by a roll angle  $(-\pi/2 < \varphi < \pi/2)$ , followed by a rotation around the  $y$  axis by a pitch angle  $(-\pi/2 < \theta < \pi/2)$ , followed by a rotation around the yaw angle  $z$  axis  $(-\pi < \psi < \pi)$ .

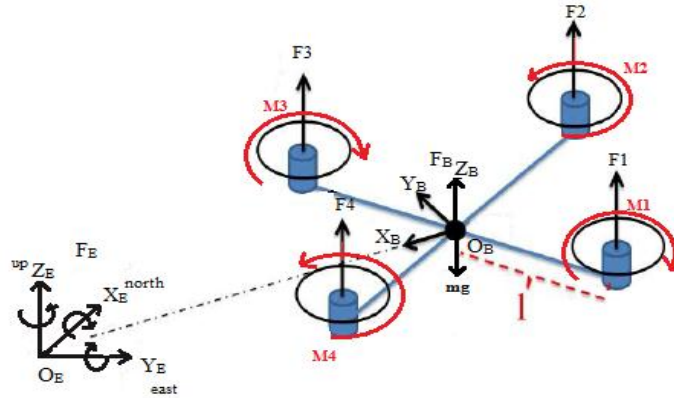


Figure (II -5): Body coordinate system

We obtain the rotation matrix using the 3 rotations according to z, according to y and according to x.

$$R = Rotx (\psi) \times Roty (\theta) \times Rotz (\varphi) \tag{2.1}$$

$$R = \begin{bmatrix} c\psi & -s\psi & 0 \\ s\psi & c\psi & 0 \\ 0 & 0 & 1 \end{bmatrix} \times \begin{bmatrix} c\theta & 0 & s\theta \\ 0 & 1 & 0 \\ -s\theta & 0 & c\theta \end{bmatrix} \times \begin{bmatrix} 1 & 0 & 0 \\ 0 & c\varphi & -s\varphi \\ 0 & s\varphi & c\varphi \end{bmatrix}$$

$$R = \begin{bmatrix} c\psi c\theta & c\psi s\theta s\varphi - s\psi c\varphi & c\psi s\theta c\varphi + s\psi s\varphi \\ s\psi c\theta & s\psi s\theta s\varphi + c\psi c\varphi & s\psi s\theta c\varphi - s\varphi c\psi \\ -s\theta & c\theta s\varphi & c\theta c\varphi \end{bmatrix} \tag{2.2}$$

With c: = cos, s:= sin

### II.3.2 Angular velocity

We express the angular velocity in the fixed frame  $\Omega_1, \Omega_2, \Omega_3$ , as a function of the angular velocity  $\dot{\varphi}, \dot{\theta}, \dot{\psi}$  in the body frame.

$$\Omega = \begin{bmatrix} \Omega_1 \\ \Omega_2 \\ \Omega_3 \end{bmatrix} = \begin{bmatrix} \dot{\varphi} \\ 0 \\ 0 \end{bmatrix} + Rotx (\varphi)^{-1} \begin{bmatrix} 0 \\ \dot{\theta} \\ 0 \end{bmatrix} + (Rot x (\varphi) Rot y (\theta))^{-1} \begin{bmatrix} 0 \\ 0 \\ \dot{\psi} \end{bmatrix} \tag{2.3}$$

The first term expresses the rotation in roll when the reference frames are matched.

The second term relates to the pitch where the rotation is expressed in the fixed reference.

The third term relates to the yaw which has already undergone two rotations where the rotation must be expressed in the fixed reference and we get:

$$\Omega = \begin{bmatrix} \Omega_1 \\ \Omega_2 \\ \Omega_3 \end{bmatrix} = \begin{bmatrix} \dot{\phi} \\ 0 \\ 0 \end{bmatrix} + \begin{bmatrix} 0 \\ \dot{\theta}c\varphi \\ -\dot{\theta}s\varphi \end{bmatrix} + \begin{bmatrix} -\dot{\psi}s\theta \\ \dot{\psi}s\varphi c\theta \\ \dot{\psi}c\varphi c\theta \end{bmatrix} \quad (2.4)$$

$$\Omega = \begin{bmatrix} 1 & 0 & -s\theta \\ 0 & c\varphi & s\varphi c\theta \\ 0 & -\varphi & c\varphi c\theta \end{bmatrix} \times \begin{bmatrix} \dot{\phi} \\ \dot{\theta} \\ \dot{\psi} \end{bmatrix} \quad (2.5)$$

Conversely:

$$\begin{bmatrix} \dot{\phi} \\ \dot{\theta} \\ \dot{\psi} \end{bmatrix} = \begin{bmatrix} 1 & s\varphi \tan\theta & c\varphi \tan\theta \\ 0 & c\varphi & -s\varphi \\ 0 & \frac{s\varphi}{c\theta} & \frac{c\varphi}{c\theta} \end{bmatrix} \times \begin{bmatrix} \Omega_1 \\ \Omega_2 \\ \Omega_3 \end{bmatrix} \quad (2.6)$$

When the quadrotor makes small rotations, we can make the following approximations:

$$c\theta = c\varphi = c\psi = 1, s\theta = s\varphi = s\psi = 0 \quad (2.7)$$

Finally we get:

$$\begin{bmatrix} \dot{\phi} \\ \dot{\theta} \\ \dot{\psi} \end{bmatrix} = \begin{bmatrix} \Omega_1 \\ \Omega_2 \\ \Omega_3 \end{bmatrix} \quad (2.8)$$

### II.3.3 Linear velocity

The linear speeds in the fixed frame are expressed as a function of the linear speeds in the moving frame by:

$$V = \begin{bmatrix} V_x^e \\ V_y^e \\ V_z^e \end{bmatrix} = R \times \begin{bmatrix} V_x^m \\ V_y^m \\ V_z^m \end{bmatrix} \quad (2.9)$$

### II.3.4 General Moments and Forces:

- **Weight force** : it is given by

$$P = mg \quad (2.10)$$

where: “m” is the total mass and “g” is gravity.

- **Thrust forces**: which are forces caused by the rotation of the motors, they are Perpendicular to the plane of the propellers.

$$F_i = b\omega_i^2 \quad (2.11)$$

With  $i=1:4$ , and “b” is the lift coefficient.

- **Drag force**: drag force is the coupling between a compressive force and the force

Viscous friction, in this case there are two drag forces acting on the system:

*The drag force in the propellers:* it acts on the blades:

$$T_h = d\omega^2 \quad (2.12)$$

Where “d” is the drag coefficient, it depends on the manufacture of the propeller.

*The drag force along the axes (x, y, and z):* It is due to the movement of the body of the quadrotor:

$$F_t = K_{ft} \cdot v \quad (2.13)$$

- **Moments due to thrust forces:**

The rotation around the x axis: it is due to the moment shouted by the difference between the forces of lift of rotors (2, 3) and (1, 4), this moment is given by the following relation:

$$M_x = \sqrt{2}/2l [(F_1 + F_4) - (F_2 + F_3)] \quad (2.14)$$

Where l is the length of the arm between the rotor and the center of gravity of the Quadrotor.

The rotation around the y axis: it is due to the moment shouted by the difference between the forces lift of rotors (1, 2) and (3, 4), this moment is given by the following relation:

$$M_y = \sqrt{2}/2l [(F_3 + F_4) - (F_1 + F_2)] \quad (2.15)$$

- **Moments due to drag forces:**

The rotation around the z axis: it is due to a reactive torque caused by the torques of Drag in each propeller, this moment is given by the following relation:

$$M_z = d (-\omega_1^2 + \omega_2^2 - \omega_3^2 + \omega_4^2) \quad (2.16)$$

Moment resulting from aerodynamic friction, it is given by:

$$M_a = K_{fa} \Omega^2 \quad (2.17)$$

- **Gyroscopic effect:**

The difficulty of changing the direction or orientation of the rotation plane of a spinning mass is known as the gyroscopic effect.

In our case there are two gyroscopic moments, the first is the propellers gyroscopic moment, the second is the gyroscopic moment due to the Quadrotor movements.

*Gyroscopic moment of the propellers:* it is given by the following relation:

$$M_{gh} = \Sigma \dot{\Omega} \wedge J_r [0 \ 0 \ (-1)^{i+1} \omega_i]^T \quad (2.18)$$

Gyroscopic moment due to Quadrotor movements: it is given by the relation:

$$M = \Omega \wedge J_r \Omega \quad (2.19)$$

### II.3.5 Development of the mathematical model

Using Newton-Euler's formulation, the equations are written in the following form:

$$\begin{cases} \dot{\zeta} = v \\ m\ddot{\zeta} = F_t + F_f + F_g \\ \dot{R} = R S(\Omega) \\ J\dot{\Omega} = -\Omega \wedge J \Omega + M_f - M_a - M_{gh} \end{cases} \quad (2.20)$$

J: inertia matrix is written in the following form:

$$\begin{bmatrix} I_x & 0 & 0 \\ 0 & I_y & 0 \\ 0 & 0 & I_z \end{bmatrix} \quad (2.21)$$

S(Ω): is the anti-symmetric matrix, for a velocity vector found in equation (2.8), it is given by:

$$S(\Omega) = \begin{bmatrix} 0 & -\Omega_3 & \Omega_2 \\ \Omega_3 & 0 & -\Omega_1 \\ -\Omega_2 & \Omega_1 & 0 \end{bmatrix} \quad (2.22)$$

F<sub>f</sub>: is the total force generated by the four rotors, it is given by:

$$F_f = R * [ 0 \quad 0 \quad \Sigma F_i ]^T \quad (2.23)$$

F<sub>t</sub>: the drag force along the axes (x, y, z), it is given by:

$$F_t = \begin{pmatrix} -k_{ftx} & 0 & 0 \\ 0 & -k_{f ty} & 0 \\ 0 & 0 & -k_{ftz} \end{pmatrix} * \dot{\zeta} \quad (2.24)$$

F<sub>g</sub>: force of gravity, it is given by:

$$F_g = \begin{bmatrix} 0 \\ 0 \\ -mg \end{bmatrix} \quad (2.25)$$



$M_f$ : moment caused by push and drag forces, it is given by:

$$M_f = \begin{bmatrix} \sqrt{2}/2 \text{ lb} [ (\omega_1^2 + \omega_4^2) - (\omega_2^2 + \omega_3^2) ] \\ \sqrt{2}/2 \text{ lb} [ (\omega_3^2 + \omega_4^2) - (\omega_1^2 + \omega_2^2) ] \\ d( -\omega_1^2 + \omega_2^2 - \omega_3^2 + \omega_4^2 ) \end{bmatrix} \quad (2.26)$$

$M_a$ : moment resulting from aerodynamic friction, it is given by:

$$M_a = \begin{bmatrix} k_{fax} \dot{\varphi}^2 \\ k_{fay} \dot{\theta}^2 \\ k_{faz} \dot{\psi}^2 \end{bmatrix} \quad (2.27)$$

### II.3.5.a Equations of translational motion:

We have:

$$m \ddot{\zeta} = F_t + F_f + F_g \quad (2.28)$$

We replace each force by its formula, we find:

$$m \begin{pmatrix} \ddot{x} \\ \ddot{y} \\ \ddot{z} \end{pmatrix} = \begin{pmatrix} \cos\varphi \sin\theta \cos\psi + \sin\psi \sin\varphi \\ \cos\varphi \sin\theta \sin\psi + \sin\varphi \cos\psi \\ \cos\varphi \cos\theta \end{pmatrix} \sum_{i=1}^4 F_i + \begin{bmatrix} -k_{ftx} & 0 & 0 \\ 0 & -k_{fty} & 0 \\ 0 & 0 & -k_{ftz} \end{bmatrix} \begin{pmatrix} \dot{x} \\ \dot{y} \\ \dot{z} \end{pmatrix} + \begin{pmatrix} 0 \\ 0 \\ -mg \end{pmatrix} \quad (2.29)$$

Then we obtain the differential equations which define the translational movement:

$$\begin{aligned} \ddot{x} &= \frac{1}{m} \left[ (\cos\varphi \sin\theta \cos\psi + \sin\psi \sin\varphi) \sum_{i=1}^4 F_i - k_{fx} \dot{x} \right] \\ \ddot{y} &= \frac{1}{m} \left[ (\cos\varphi \sin\theta \sin\psi + \sin\varphi \cos\psi) \sum_{i=1}^4 F_i - k_{fy} \dot{y} \right] \\ \ddot{z} &= \frac{1}{m} \left[ (\cos\varphi \cos\theta) \sum_{i=1}^4 F_i - k_{fz} \dot{z} \right] - g \end{aligned} \quad (2.30)$$

II.3.5.b Equations of rotational motion:

We have:

$$J\dot{\Omega} = -\Omega \wedge J\Omega - M_{gh} - M_a + M_f \quad (2.31)$$

We replace each moment by the corresponding formula, we find:

$$\begin{bmatrix} I_x & 0 & 0 \\ 0 & I_y & 0 \\ 0 & 0 & I_z \end{bmatrix} \begin{pmatrix} \ddot{\phi} \\ \ddot{\theta} \\ \ddot{\psi} \end{pmatrix} = - \begin{pmatrix} \dot{\phi} \\ \dot{\theta} \\ \dot{\psi} \end{pmatrix} \wedge \left( \begin{bmatrix} I_x & 0 & 0 \\ 0 & I_y & 0 \\ 0 & 0 & I_z \end{bmatrix} \begin{pmatrix} \dot{\phi} \\ \dot{\theta} \\ \dot{\psi} \end{pmatrix} \right) - \begin{pmatrix} J_r \overline{\Omega_r} \dot{\theta} \\ J_r \overline{\Omega_r} \dot{\phi} \\ 0 \end{pmatrix} - \begin{pmatrix} k_{fax} \dot{\phi}^2 \\ k_{fay} \dot{\theta}^2 \\ k_{faz} \dot{\psi}^2 \end{pmatrix} + \begin{pmatrix} \sqrt{2}/2 \text{ lb} [(\omega_1^2 + \omega_4^2) - (\omega_2^2 + \omega_3^2)] \\ \sqrt{2}/2 \text{ lb} [(\omega_3^2 + \omega_4^2) - (\omega_1^2 + \omega_2^2)] \\ d(-\omega_1^2 + \omega_2^2 - \omega_3^2 + \omega_4^2) \end{pmatrix} \quad (2.32)$$

Then we obtain the differential equations defining the rotational movement:

$$\begin{aligned} I_x \ddot{\phi} &= -\dot{\theta}\dot{\psi}(I_z - I_y) - J_r \overline{\Omega_r} \dot{\theta} - k_{fax} \dot{\phi}^2 + \frac{\sqrt{2}}{2} \text{ lb} [(\omega_1^2 + \omega_4^2) - (\omega_2^2 + \omega_3^2)] \\ I_y \ddot{\theta} &= \dot{\phi}\dot{\psi} (I_z - I_x) + J_r \overline{\Omega_r} \dot{\phi} - k_{fay} \dot{\theta}^2 + \frac{\sqrt{2}}{2} \text{ lb} [(\omega_3^2 + \omega_4^2) - (\omega_1^2 + \omega_2^2)] \\ I_z \ddot{\psi} &= -\dot{\phi}\dot{\theta} (I_y - I_x) - k_{faz} \dot{\psi}^2 + d(-\omega_1^2 + \omega_2^2 - \omega_3^2 + \omega_4^2) \end{aligned} \quad (2.33)$$

Where  $\overline{\Omega_r}$  defines the overall propellers' speed [rad s<sup>-1</sup>]

$$\overline{\Omega_r} = -\omega_1 + \omega_2 - \omega_3 + \omega_4 \quad (2.34)$$

The complete dynamic model that governs the quadrotor is as follows:

$$\begin{cases} \ddot{\phi} = \frac{\dot{\theta}\dot{\psi} (I_y - I_z)}{I_x} - \frac{J_r}{I_x} \overline{\Omega_r} \dot{\theta} - \frac{k_{fax}}{I_x} \dot{\phi}^2 + \frac{\sqrt{2}}{2 I_x} l U_2 \\ \ddot{\theta} = \frac{\dot{\phi}\dot{\psi} (I_z - I_x)}{I_y} + \frac{J_r}{I_y} \overline{\Omega_r} \dot{\phi} - \frac{k_{fay}}{I_y} \dot{\theta}^2 + \frac{\sqrt{2}}{2 I_y} l U_3 \\ \ddot{\psi} = \frac{\dot{\phi}\dot{\theta} (I_x - I_y)}{I_z} - \frac{k_{faz}}{I_z} \dot{\psi}^2 + \frac{U_4}{I_z} \end{cases} \quad (2.35)$$

$$\begin{cases} \ddot{x} = \frac{-k_{fx}}{m} \dot{x} + \frac{1}{m} U_x U_1 \\ \ddot{y} = -\frac{k_{fy}}{m} \dot{y} + \frac{1}{m} U_y U_1 \\ \ddot{z} = \frac{-k_{fz}}{m} \dot{z} - g + \frac{(\cos\varphi \cos\theta)}{m} U_1 \end{cases}$$

$$U = [U_1 \ U_2 \ U_3 \ U_4]^T \quad (2.36)$$

Where the commands are expressed as follows:

$$U_1 = b(\omega_1^2 + \omega_2^2 + \omega_3^2 + \omega_4^2)$$

$$U_2 = b(\omega_1^2 - \omega_2^2 - \omega_3^2 + \omega_4^2)$$

$$U_3 = b(-\omega_1^2 - \omega_2^2 + \omega_3^2 + \omega_4^2)$$

$$U_4 = d(-\omega_1^2 + \omega_2^2 - \omega_3^2 + \omega_4^2) \quad (2.37)$$

$$\begin{cases} U_x = \cos\varphi \sin\theta \cos\psi + \sin\psi \sin\varphi \\ U_y = \cos\varphi \sin\theta \sin\psi - \sin\varphi \cos\psi \end{cases} \quad (2.38)$$

### II.3.6 Rotor dynamics

Many motion control applications use permanent magnet DC motors. Since it is easier to implement control systems using DC motors compared to AC motors, they are often used when speed, torque, or position needs to be controlled. [11]

Brushed motors and brushless motors are the two most popular types of DC motors. The rotor permanent magnet of a brushless DC motor is powered by the magnetic force of the stator's winding circuit. The brushless DC motor utilizes a sensor and an electronic circuit for current switching, whereas the brush DC motor uses a brush and switch.

Both BLDC and Brushed motors work using the same attraction and repulsion principles between coils and permanent magnets. Where, the dynamics of a brushless DC motor at steady state is the same as a conventional DC motor. [12]

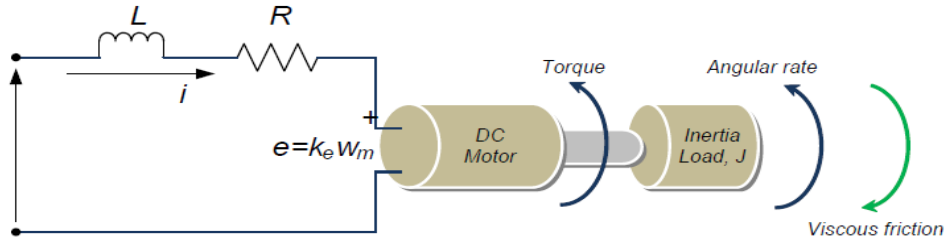


Figure (II-6): brushless DC motor schematic at steady state

The circuit above contains an internal resistance  $R$ , an internal inductance  $L$  and the electromagnetic force obtained from the rotor.

By using the law of KIRCHOFF KVL (Kirchhoff's voltage law), we obtain the following equation:

$$V_s = Ri + L \frac{di}{dt} + e \quad (2.43)$$

From the Newton's second law of motion, we get the mechanical properties relative to the torque of the system arrangement would be the product of the Inertia load  $J$ , and the rate of angular velocity  $\omega_m$  is equal to the sum of all the torques. These follow with equation:

$$J (d\omega_m)/dt = \Sigma T_i$$

$$T_e = K_f \omega_m + J \frac{d\omega_m}{dt} + T_L \quad (2.44)$$

Where the electrical torque and the back emf are respectively equal to:

$$e = K_e \omega_m \quad (2.45)$$

$$T_e = K_t \omega_m \quad (2.46)$$

Therefore, we obtain:

$$\frac{di}{dt} = -i \frac{R}{L} - \frac{K_e}{L} \omega_m + \frac{1}{L} V_s \quad (2.47)$$

$$\frac{d\omega_m}{dt} = i \frac{K_t}{J} - \frac{K_f}{J} \omega_m + \frac{1}{J} T_l \quad (2.48)$$

Using the Laplace Transform to evaluate the two above equations, the following are obtained appropriately (all initial conditions are assumed to be zero):

$$L \left\{ \frac{di}{dt} = -i \frac{R}{L} - \frac{K_e}{L} \omega_m + \frac{1}{L} V_s \right\} \quad (2.49)$$

This implies:

$$si = -i \frac{R}{L} - \frac{K_e}{L} \omega_m + \frac{1}{L} V_s$$

$$L \left\{ \frac{d\omega_m}{dt} = -i \frac{k_t}{J} - \frac{k_f}{J} \omega_m + \frac{1}{J} T_L \right\}$$

$$s\omega_m = i \frac{K_t}{J} - \frac{K_f}{J} \omega_m + \frac{1}{J} T_L \quad (2.50)$$

At no load (for  $T_L = 0$ ):

$$s\omega_m = i \frac{K_t}{J} - \frac{K_f}{J} \omega_m \quad (2.51)$$

From this equation we get:

$$i = \frac{s\omega_m + \frac{K_f}{J} \omega_m}{\frac{K_t}{J}}$$

$$\left( \frac{s\omega_m + \frac{K_f}{J} \omega_m}{\frac{K_t}{J}} \right) \left( s + \frac{R}{L} \right) = -\frac{K_e}{L} \omega_m + \frac{1}{L} V_s$$

$$V_s = \left\{ \frac{\{s^2\}L + sK_fL + sRJ + K_fR + K_eK_t}{K_t} \right\} \omega_m \quad (2.52)$$

The transfer function is therefore obtained as follows using the ratio of the angular velocity,  $\omega_m$  to source voltage  $V_s$ :

$$G(s) = \frac{\omega_m}{V_s} = \left\{ \frac{K_t}{\{s^2\}L + sK_fL + sRJ + K_fR + K_eK_t} \right\} \quad (2.53)$$

We consider: the friction constant as small that  $K_f$  tends to 0 and we get:

$$K_e K_t \gg R K_f \text{ and } R J \gg K_f L$$

Last but not least the transfer function becomes:

$$G(s) = \frac{\omega_m}{V_s} = \left\{ \frac{K_t}{\{s^2 J L + s R J + K_e K_t\}} \right\} \quad (2.54)$$

Where the mechanical time constant is equal to:

$$\tau_m = \frac{R J}{K_e K_t} \quad (2.55)$$

And the electrical time constant is equal to:

$$\tau_e = \frac{L}{R} \quad (2.56)$$

Finally the transfer function is rewritten then as follow:

$$G(s) = \frac{\omega_m}{V_s} = \left\{ \frac{\frac{1}{K_e}}{\tau_m \cdot \tau_e \cdot s^2 + \tau_m \cdot s + 1} \right\} \quad (2.57)$$

Since we are working with the BLDC which is presented in the following figure with star assembly and three phases the equations becomes:

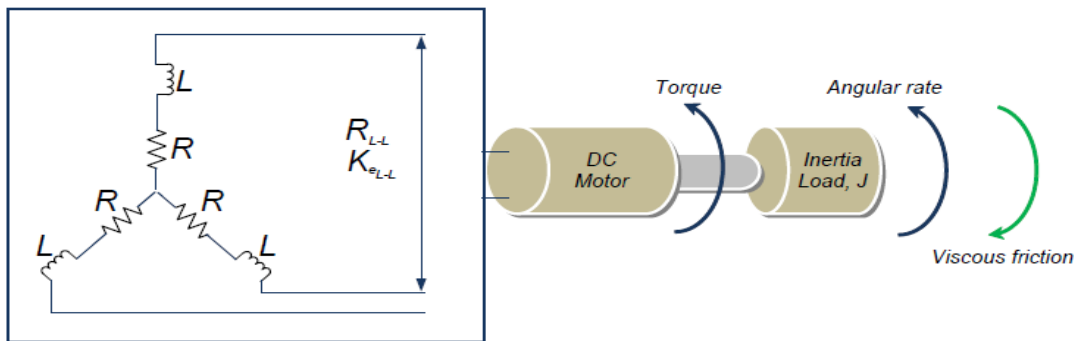


Figure (II -7): Star assembly of BLDC motor

Mechanical constant:

$$\tau_m = \frac{3 \cdot R J}{K_e K_t} \quad (2.58)$$

Electrical constant:

$$T_e = \frac{L}{3 \cdot R} \tag{2.59}$$

Considering the phase shift effect:

$$T_m = \frac{3 \cdot R \cdot J}{K_e \cdot K_t} \tag{2.60}$$

Therefore, the equation for the BLDC can now be obtained as follow by considering the effects of the constants and the phase accordingly.

$$G(s) = \left\{ \frac{\frac{1}{K_e}}{T_m \cdot T_e \cdot S^2 + T_m \cdot S + 1} \right\} \tag{2.61}$$

**Numerical application**

**Table (II -1): 1000kv BLDC parameters**

Parameters	Value	Unit
Rotor mass	26.35	G
Motor constant	1000	Kv
Motor efficiency	80	%
Motor diameter	28	Mm
Motor poles	14	
Wire resistance	0.09	Ω
Wire diameter	0.25	mm
Prop diameter	203.2	mm
Prop chord	114	mm
Prop mass	5.5	G

$$G(s) = \frac{83.7758}{8.6808 \cdot 10^{-10} S^2 + 0.0017223 S + 1} \tag{2.61}$$

**II.4 Conclusion**

In this chapter we have described the basic movements of the quadrotor, mathematical modeling quadrotor type in (X) mode at six degrees of freedom. The model is developed on the basis of the formalism Newton-Euler.

The complete model includes almost all the physical phenomena acting on the quadrotor during the flight. From the modeling obtained, we were able to conclude that the quadrotor is complex, nonlinear system and under actuated system. The control part of the flying machine will be discussed in the next chapter.



# **Chapter III:**

## **Quadrotor Identification and Control**

### **III.1 Introduction**

The flight control system is the core of the UAV. In order to complete the autonomous flight, the UAV requires the control system to have stability and good control characteristics for the internal loop (attitude loop) and outer loop (horizontal position and height loop).

There are several control Techniques, starting with intelligent control which has advanced significantly in theory and applied technologies in recent years for example, Neural Networks (NN), Genetic Algorithms, Fuzzy Logic, and Particle Swarm Optimization (PSO) methods can be used to solve several complex engineering problems. However, they usually involve a great deal of uncertainty and mathematical complexity, and the controller's structure grows more complicated as a result. Also, we have got nonlinear control methods that are usually classified as model-based nonlinear control methods, including Integral Sliding Mode Control (ISMC), Back-stepping Control, Adaptive control and Active Disturbance Rejection Control (ADRC). Finally, most of aircrafts are based on linear flight control theory such as Linear Quadratic Regulator (LQR),  $H^\infty$  controller and Proportional Integrator Derivative controller (PID) that will be explained in details in the next section.

### **III.2 Parameters Identification**

The Quadrotor vehicle was disassembled into individual components to measure the moment of inertia. Each component was modelled using a reduced geometric form with a constant internal density. The weight of each component was then determined. The vehicle's total moment of inertia matrix is the sum of the inertias for each component around each axis.

The next section, shows the basic measurements done in the identification process.

#### **III.2.1 Total mass**

We used an electronic balance to weigh the quadrotor, after finishing the assembly and wiring of it, we found that our drone weighs 0.950 [kg].



**Figure (III -1):** Balance for measuring quadrotor mass

Remark: For measuring the length and dimensions of the quadrotor we used a tape.

### III.2.2 Inertia matrix "I"

There are two methods to determine the inertia parameters:

The first one is the practical method, it is called the bifilar pendulum experiment: [13]

In this experiment the quadrotor body is held by two chords. The aim of this experiment, is to measure the period of oscillation, to calculate the inertia of the quadrotor using following equation:

$$I = \frac{mgT^2r}{4\pi^2L} \quad (3.1)$$

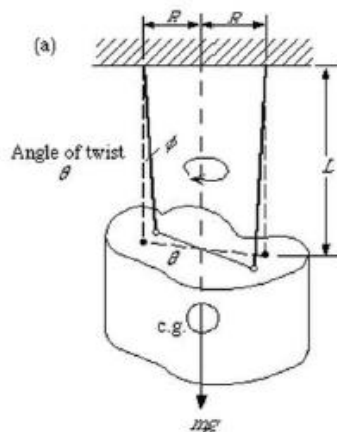


**Figure (III -2):** The bifilar pendulum experiment

For  $I_{xx}$ , the experiment consists in keeping the two chords in the equilibrium position in the vertical plane. Then we apply a rotation in the horizontal plane with any angle and we release.

For  $I_{yy}$ , the experiment is repeated by rotating the drone by  $\pm 90^\circ$  in the vertical plane. The rest of the experience is the same.

For  $I_{zz}$ , the quadrotor is kept in balance between the two chords at the position horizontal. Then for the same procedure as previous is applied.

The second method is theoretical, in this project we used this method, and the structure of the quadrotor has to be modeled as components with easier geometry. The body of inertia tensor may be reduced as a diagonal matrix due to the high degree of symmetry in the structure: [14], [15]

One cross structure (Arms) modeled as two solid narrow cylinders fastened in the middle forming a cross, one electronics box modeled as a rectangular parallelepiped, four motors modeled as solid cylinders, four motor gears modeled as solid cylinders, four propellers modeled as flat cylinders.

#### *The cross structure (Arms)*

A cylindrical rods configuration was used to measure the moment of inertia for the arms. Figure (III.3) and Equations (3.2) were used to calculate the mass moment of inertia for the arms. The narrow cylinders of the cross structure model have a radius  $R_c$  of  $4 \cdot 10^{-3}$  [m], a length  $L_c$  of 0.43 [m] and a mass  $M_c$  of 0.238 [kg] each.

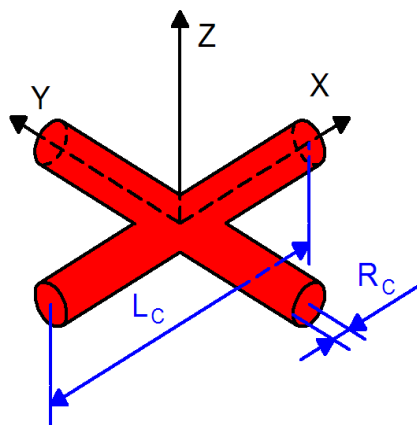


**Figure (III -3):** *cross structure identification*

The cross structure moment of inertia around the x-axis  $I_{cx}$  [N m s<sup>2</sup>] is equal to that one around the y-axis  $I_{cy}$  [N m s<sup>2</sup>] (thanks to the symmetry):

$$\begin{aligned}
 I_{cx} &= I_{cy} = M_c * \left( \frac{R_c^2}{4} + \frac{L_c^2}{12} \right) + \frac{1}{2} * M_c * R_c^2 \\
 I_{cx} &= I_{cy} = 3.859 * 10^{-3} \text{ (N m s}^2\text{)} \\
 I_{cz} &= M_c * \left( \frac{R_c^2}{4} + \frac{L_c^2}{12} \right) + M_c * \left( \frac{R_c^2}{4} + \frac{L_c^2}{12} \right) \\
 I_{cz} &= 7.336 * 10^{-3} \text{ (N m s}^2\text{)} \tag{3.2}
 \end{aligned}$$

*The central hub*

The central hub was represented as a rectangular parallelepiped, and the central hub's mass moment of inertia was calculated using Figure (III.4) equations (3.3). It has a length  $L_E = 0.181$  m , a width  $W_E = 0.108$  m , a height  $H_E = 0.04$  m , a distance from the COM around the z-axis  $D_E = 60 * 10^{-3}$  m , and a mass  $M_E = 0.208$  kg.

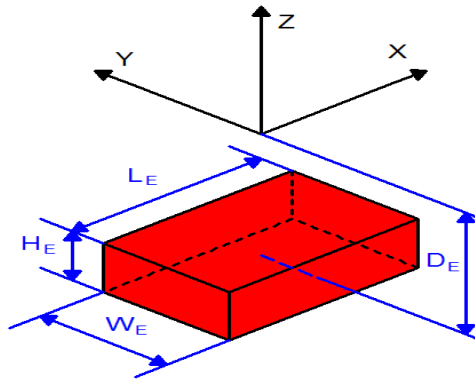


**Figure (III -4):** The rectangular parallelepiped identification

We used the formula of parallelepiped inertia:

$$\begin{aligned}
 I_{Ex} &= M_E \left( \frac{W_E^2}{12} + \frac{H_E^2}{12} + D_E^2 \right) = 9.79 * 10^{-4} \text{ (N m s}^2\text{)} \\
 I_{Ey} &= M_E \left( \frac{L_E^2}{12} + \frac{H_E^2}{12} + D_E^2 \right) = 9.28 * 10^{-4} \text{ (N m s}^2\text{)} \\
 I_{Ez} &= M_E \left( \frac{L_E^2}{12} + \frac{W_E^2}{12} \right) = 7.7 * 10^{-4} \text{ (N m s}^2\text{)} \tag{3.3}
 \end{aligned}$$

The four motors:

The solid cylinder of the motor model has a radius  $R_M = 0.014$  m, a height  $H_M = 40 \cdot 10^{-3}$  m, a distance from the COM around the x-axis  $L_M = 210 \cdot 10^{-3}$  m, a distance from the COM around the z-axis  $D_M = 12 \cdot 10^{-3}$  m and a mass  $M_M = 0.059$  kg.

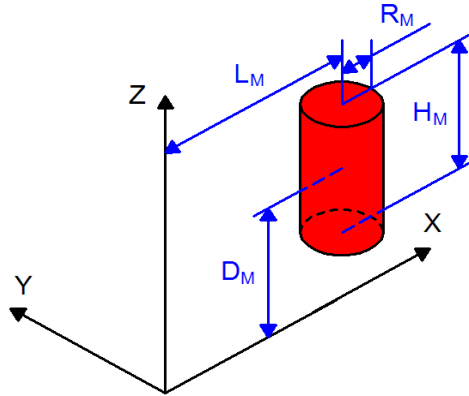


Figure (III -5): The motors identification

We used the formula of cylinder inertia we find:

$$\begin{aligned}
 I_{M1x} &= M_M \left( \frac{R_M^2}{4} + \frac{H_M^2}{12} + D_M^2 \right) = 1.93 \cdot 10^{-5} \text{ (N m s}^2\text{)} \\
 I_{M1y} &= M_M \left( \frac{R_M^2}{4} + \frac{H_M^2}{12} + L_M^2 + D_M^2 \right) = 2.62 \cdot 10^{-3} \text{ (N m s}^2\text{)} \\
 I_{M1z} &= M_M \left( \frac{R_M^2}{2} + L_M^2 \right) = 2.6 \cdot 10^{-3} \text{ (N m s}^2\text{)}
 \end{aligned} \tag{3.4}$$

The four motors show a high degree of symmetry, therefore the computation were done just on the front motor and then transposed on the other ones, so we have:

$$\begin{aligned}
 I_{M1x} &= I_{M2x} = I_{M3x} = I_{M4x} \\
 I_{M1y} &= I_{M2y} = I_{M3y} = I_{M4y} \\
 I_{M1z} &= I_{M2z} = I_{M3z} = I_{M4z}
 \end{aligned} \tag{3.5}$$

*Propellers:*

The four propellers have been modeled as flat cylinders with variable density. This shape has been chosen because it comes from a rotating (flat plate) propeller, furthermore the density depends on the radius and it decreases by getting far from the center. [14]

The flat cylinder of the propeller model has a radius  $R_p = 101.6 \cdot 10^{-3}$  m, a height  $H_p = 10 \cdot 10^{-3}$  m, a distance from the COM around the x-axis  $L_p = 210 \cdot 10^{-3}$  m, a distance from the COM around the z-axis  $D_p = 33 \cdot 10^{-3}$  m and a mass  $M_p = 5,5 \cdot 10^{-3}$  kg.

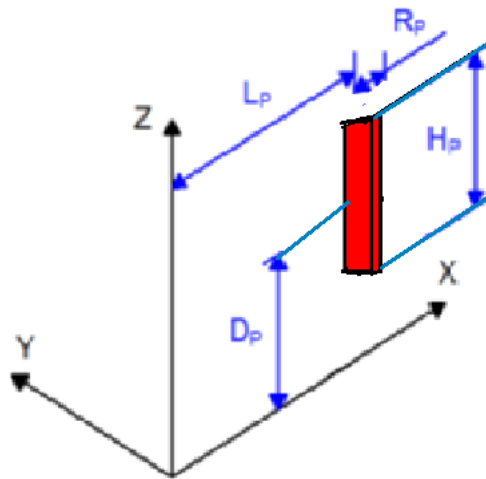


**Figure (III -6):** *Propellers identification*

We used the formula of the flat cylinder inertia we find:

$$\begin{aligned}
 I_{p1x} &= M_p \left( \frac{R_p^2}{6} + \frac{H_p^2}{12} + D_p^2 \right) = 1.55 \cdot 10^{-5} \quad (N m s^2) \\
 I_{p1y} &= M_p \left( \frac{R_p^2}{6} + \frac{H_p^2}{12} + L_p^2 + D_p^2 \right) = 2.58 \cdot 10^{-4} \quad (N m s^2) \\
 I_{p1z} &= M_p \left( \frac{R_p^2}{3} + L_p^2 \right) = 2.62 \cdot 10^{-4} \quad (N m s^2)
 \end{aligned} \tag{3.6}$$

The four propellers show a high degree of symmetry, therefore the computation were done just on the front propeller and then transposed on the other ones, so we have:

$$\begin{aligned}
 I_{p1x} &= I_{p2x} = I_{p3x} = I_{p4x} \\
 I_{p1y} &= I_{p2y} = I_{p3y} = I_{p4y} \\
 I_{p1z} &= I_{p2z} = I_{p3z} = I_{p4z}
 \end{aligned} \tag{3.7}$$

*Motor gears:*

The motors were modelled as a solid cylinders to determine the mass moment of inertia for all four motors.

The solid cylinder of the motor gear model has a radius  $R_{MG} = 4 \cdot 10^{-3}$  m, a height  $H_{MG} = 10 \cdot 10^{-3}$  m, a distance from the COM around the x-axis  $L_{MG} = 210 \cdot 10^{-3}$  m, a distance from the COM around the z-axis  $D_{MG} = 43 \cdot 10^{-3}$  m and a mass  $M_{MG} = 1.1 \cdot 10^{-3}$  kg.

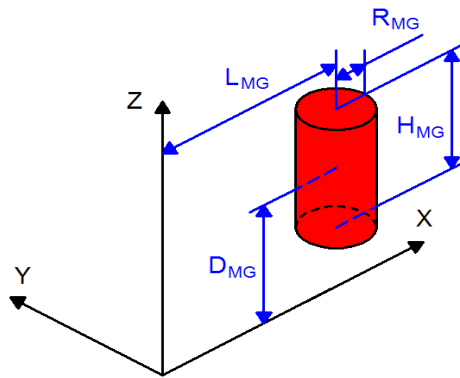


**Figure (III -7):** Motor gear identification.

We used the formula of cylinder inertia we find:

$$\begin{aligned}
 I_{MG1x} &= M_{MG} \left( \frac{R_{MG}^2}{4} + \frac{H_{MG}^2}{12} + D_{MG}^2 \right) = 2.05 \cdot 10^{-6} \quad (N \ m \ s^2) \\
 I_{MG1y} &= M_{MG} \left( \frac{R_{MG}^2}{4} + \frac{H_{MG}^2}{12} + L_{MG}^2 + D_{MG}^2 \right) = 5.05 \cdot 10^{-5} \quad (N \ m \ s^2) \\
 I_{MG1z} &= M_{MG} \left( \frac{R_{MG}^2}{2} + L_{MG}^2 \right) = 4.85 \cdot 10^{-5} \quad (N \ m \ s^2)
 \end{aligned} \tag{3.8}$$



The four motor gears show a high degree of symmetry, therefore the computation were done just on the front propeller and then transposed on the other ones, so we have:

$$\begin{aligned}
 I_{MG1x} &= I_{MG2x} = I_{MG3x} = I_{MG4x} \\
 I_{MG1y} &= I_{MG2y} = I_{MG3y} = I_{MG4y} \\
 I_{MG1z} &= I_{MG2z} = I_{MG3z} = I_{MG4z}
 \end{aligned} \tag{3.9}$$

This is how it looks motor +propeller + motor gear:

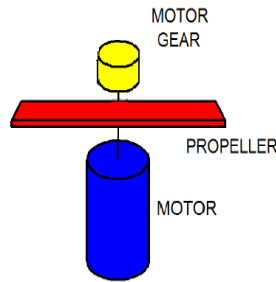


**Figure (III -8):** Motor propeller motor gear assembly identification.

Now, it is possible to compute the three body moment of inertia  $I_{xx}$ ,  $I_{yy}$  and  $I_{zz}$  by adding all the components around a defined axis.

$$\begin{aligned}
 I_{xx} &= I_{cx} + I_{Ex} + 4 * I_{M1x} + 4 * I_{MG1x} + 4 * I_{p1x} = 5 * 10^{-3} [N ms^2] \\
 I_{yy} &= I_{cy} + I_{Ey} + 4 * I_{M1y} + 4 * I_{MG1y} + 4 * I_{p1xy} = 5 * 10^{-3} [N ms^2] \\
 I_{zz} &= I_{cz} + I_{Ez} + 4 * I_{M1z} + 4 * I_{MG1z} + 4 * I_{p1z} = 19.8 * 10^{-3} [N ms^2]
 \end{aligned} \tag{3.10}$$

### III.2.3 Lift coefficient “b”

The coefficient of lift b is proportional to the square of the speed of rotation of the motor. [16]

At  $\omega=1243\text{pwm}$ , where  $\omega = 823.306\text{rad/s}$  and  $m=0.7$  kg (without battery)

We have:

$$P = F_i \quad (3.11)$$

$$m g = 4 * b * \omega^2 \quad (3.12)$$

$$b = \frac{m g}{4 \omega^2} = \frac{0.7 * 9.8}{4 * (823.603)^2} = 2.52 * 10^{-6} \quad (3.13)$$

### III.2.4 drag coefficient “d”

According to aerodynamic theory, the drag coefficient depends on the coefficient lift with the following relation. [29]

$$\frac{d}{b} = \tan \alpha \quad (3.14)$$

Where  $\alpha = 20^\circ$  is the angle of incidence of the propeller formed by the propeller body and the draft.

$$d = b * \tan \alpha = 2.52 * 10^{-6} * \tan (20^\circ) = 9.17 * 10^{-7} \quad (3.15)$$

We organize the results in the following table:

**Table (III -1):** *Quadr parameters obtained by identification*

Parameters	Measure
$I_{xx}$	$5 * 10^{-3}$ [N ms <sup>2</sup> ]
$I_{yy}$	$5 * 10^{-3}$ [N ms <sup>2</sup> ]
$I_{zz}$	$19.8 * 10^{-3}$ [N ms <sup>2</sup> ]
b	$2.52 * 10^{-6}$
d	$9.17 * 10^{-7}$
$J_r$	$3.0009 * 10^{-5}$ [N ms <sup>2</sup> ]
M	950 [g]

### III.3 State estimation

State estimation is one of the fundamental problems in the study of autonomous control systems. Precise state estimation is a necessary condition for effective control; it allows a system to have accurate knowledge of its current state and, consequently, to make informed decisions when choosing future control inputs. At a high level, the state estimation filtering problem is as follows. The system in question would like to achieve a certain goal (e.g., reach a destination); to do this, the system needs to know its state (attitude in our case) in order to apply the necessary control inputs. To compute its state, the system has access to measurements (e.g., IMU) of its state; the system's goal is to use all of its available information about its sensor models and about its own dynamics in order to obtain a precise estimate of its state. [17]

In this work, we explore the madgwick filter used in the MPU code.

#### Madgwick filter

Madgwick filter is a complementary filter in which the accelerometer and the magnetometer measurements are fused by means of a gradient descent algorithm. For the magnetic readings, only the horizontal projection is used to correct the orientation. The fusion process is governed by a unique parameter: [18]

$\beta$  : inverse gyroscope weight

The filter consists of a cluster of a tri-axis accelerometer, a tri-axis magnetometer, and a tri-axis angular rate sensor. The proposed filter implementation incorporates gyroscope bias drift compensation.

The filter performs the calculations of rotations using quaternions rather than Euler angles, which avoids the singularities issue associated with attitude estimation. The accelerometer and magnetometer are calibrated off-line prior to the data fusion process. The magnetometer calibration is made using the ellipsoid fitting technique. Experimental validation of the filter with the actual sensor data proved to be satisfactory. [19]

Most of the recent sensor fusion algorithms for inertial or magnetic sensors, are designed to perform the orientation estimation in quaternion form. Quaternions are part of a powerful mathematical tool which requires less computation time because of their minimal number of parameters. [20], [21]

Additionally, they avoid the singularity configurations unlike the Euler representation. Where the quaternions initial conditions are (1, 0, 0, 0). The equations of three angles using quaternions:

$$\text{Yaw} = \text{atan2}(2 * (q_1 * q_2 + q_0 * q_3), q_0 * q_0 + q_1 * q_1 - q_2 * q_2 - q_3 * q_3)$$

$$\text{Roll} = \text{atan2}(-2 * (q_0 * q_1 + q_2 * q_3), -1 * (q_0 * q_0 - q_1 * q_1 - q_2 * q_2 + q_3 * q_3))$$

$$\text{Pitch} = \text{asin}(2 * (q_1 * q_3 - q_0 * q_2)) \tag{3.16}$$

In the next figure, we present the Madgwick filter and IMU operating diagram:

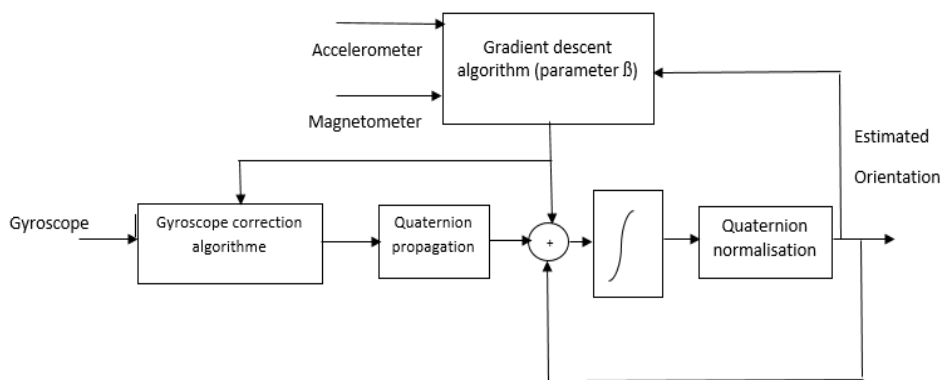


Figure (III -9): MPU operating diagram

Vibrations, distribution of inertia are the main reasons of IMU imbalance.

Before we start talking about the madgwick filter formulation, let us formally define coordinate axes we will use. Let the letters I, W, B denote inertial, world and body frames respectively. Generally B and I are the same but they don't have to be. [22]

In quaternion space, the Madgwick filter formulates the attitude estimation issue. The general idea of the Madgwick filter is to estimate  ${}^I_W q_{t+1}$  by fusing/combining attitude estimates by integrating gyro measurements  ${}^I_\omega q_\omega$  and direction obtained by the accelerometer measurements.

As in Complementary Filter, the attitude is estimated from the gyro by numerical integration. [23]

The attitude estimation from the accelerometer is done by using a gradient descent algorithm to solve the following minimization problem:

$$\min_{\hat{q} \in \mathbb{R}^{4 \times 1}} f(\hat{q}, W_{\hat{g}}, I_{\hat{a}}) \quad (3.17)$$

$$f(\hat{q}, W_{\hat{g}}, I_{\hat{a}}) = \hat{q}^* \otimes W_{\hat{g}} \otimes \hat{q} - I_{\hat{a}} \quad (3.18)$$

Here,  $q^*$  denotes the conjugate of  $q$  and  $\otimes$  indicates quaternion multiplication.  $W_{\hat{g}}$  Denotes the normalized gravity vector and is given by  $W_{\hat{g}}=[0001]^T$  and  $I_{\hat{a}}$  denotes the normalized acceleration measurements. Following are the steps for attitude estimation using a Madgwick filter: [23]

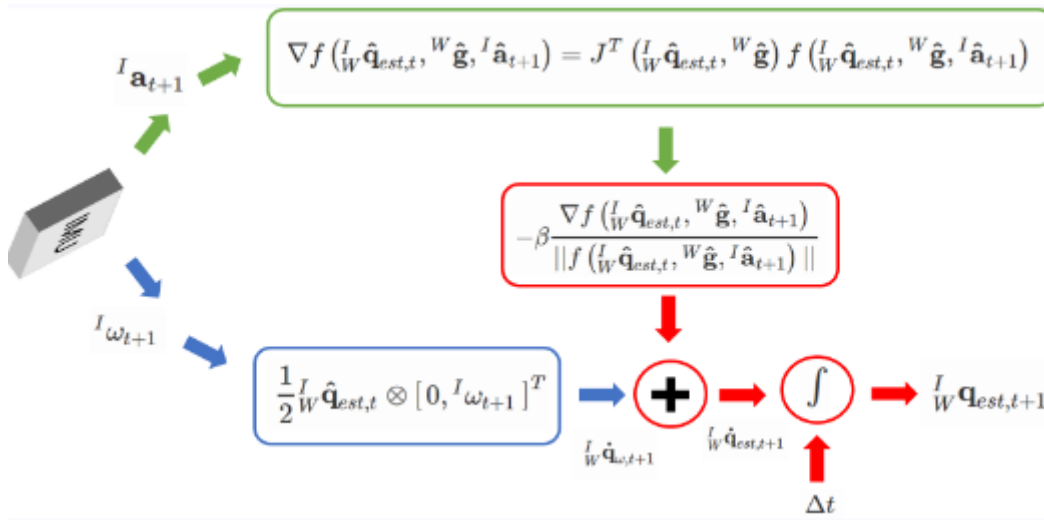


**Figure (III -10):** Overview of Madgwick Filter

**Step 1:** Obtain sensor measurements

Obtain gyro and accelerometer measurements from the sensor. Let  $I_{\omega_t}$  and  $I_{\hat{a}_t}$  denote the gyro and accelerometer measurements respectively. Also,  $I_{\hat{a}_t}$  refers to the normalized accelerometer measurements.

**Step 2.a:** Orientation increment from Accelerometer

Compute orientation increment from accelerometer measurements (gradient step).

$$\nabla f({}^I\hat{q}_{est,t}, W_{\hat{g}}, I_{\hat{a}_{t+1}}) = J^T({}^I\hat{q}_{est,t}, W_{\hat{g}}) f({}^I\hat{q}_{est,t}, W_{\hat{g}}, I_{\hat{a}_{t+1}}) \quad (3.19)$$

$$f({}^I\hat{q}_{est,t}, W_{\hat{g}}, I_{\hat{a}_{t+1}}) = \begin{pmatrix} 2(q_2q_4 - q_1q_3) - a_x \\ 2(q_1q_2 + q_3q_4) - a_y \\ 2(\frac{1}{2} - q_2^2 - q_3^2) - a_z \end{pmatrix} \quad (3.20)$$

$$J({}^I\hat{q}_{est,t}, W_{\hat{g}}) = \begin{bmatrix} -2q_3 & 2q_4 & -2q_1 & 2q_2 \\ 2q_2 & 2q_1 & 2q_4 & 2q_3 \\ 0 & -4q_2 & -4q_3 & 0 \end{bmatrix} \quad (3.21)$$

Update Term (Attitude component from accelerometer measurements) is given by:

$${}^Iq_{\nabla,t+1} = -\beta \frac{\nabla f({}^I\hat{q}_{est,t}, W_{\hat{g}}, I_{\hat{a}_{t+1}})}{\|f({}^I\hat{q}_{est,t}, W_{\hat{g}}, I_{\hat{a}_{t+1}})\|} \quad (3.22)$$

**Step 2.b:** Orientation increment from gyro:

Compute orientation increment from gyro measurements (numerical integration).

$${}^I\hat{q}_{est,t+1} = \frac{1}{2} {}^I\hat{q}_{est,t} \otimes [0, I_{\omega_{t+1}}]^T \quad (3.23)$$

**Step 3:** Fuse Measurements

Fuse the measurements from both the accelerometer and gyro to obtain the estimated attitude  ${}^I\hat{q}_{est,t+1}$ :

$${}^I\hat{q}_{est,t+1} = {}^I\hat{q}_{est,t} + {}^I\hat{q}_{est,t+1}\Delta t \quad (3.24)$$

Here,  $\Delta t$ : is the time elapsed between two samples at  $t$  and  $t+1$ . Repeat steps 1 to 3 for every time instant.

**Remark:** The user must define the initial estimations of the attitude, biases, and sample duration in a Madgwick filter. The initial attitude can be assumed to be zero if it has to be obtained by external sources such as a motion capture system.

### III.4 Control system architecture design

We designed a control system architecture for hovering and stabilizing the quadrotor presented in figure (III.11), in the next section we are going to detail each block of this diagram starting with the quadrotor Model:

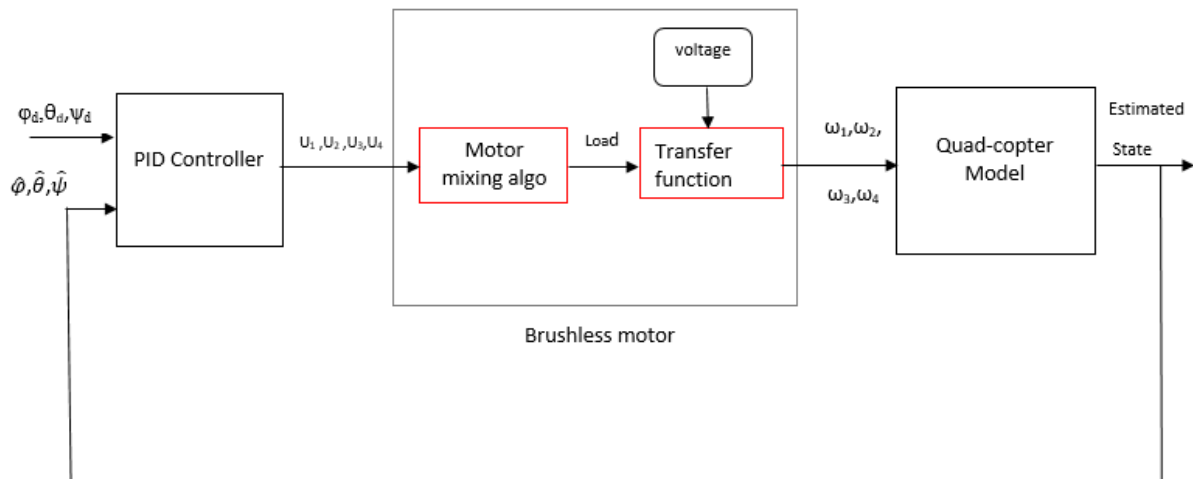


Figure (III -11): control system architecture

#### III.4.1 Quadrotor modelling for control

As we can see from the structure above, the drone takes four motors speed as inputs which then spin the propellers generating forces and torques that affect the output state that hover the drone (which means  $\varphi, \theta, \psi$ ), these four motors was commanded manually with a potentiometer in the emission part.

The dynamic model of our UAV presented before contains two gyroscopic effects. The influence of these effects is in our case less important than the motor's action. Particularly in the case of a near-hover situation. [25]

In order to make it possible to design multiple PID controllers for this system, we use the low angle theorem and the negligible drag force assumption so the equations can be simplified. The system is rewritten then as follows:

$$\begin{cases} \ddot{x} = \frac{1}{m} U_x U_1 \\ \ddot{y} = \frac{1}{m} U_y U_1 \\ \ddot{z} = -g + \frac{(\cos\varphi \cos\theta)}{m} U_1 \end{cases} \quad (3.25)$$

$$\begin{cases} \ddot{\varphi} = a_1 \dot{\psi} \dot{\theta} + a_2 \overline{\Omega_r} \dot{\theta} + b_1 U_2 \\ \ddot{\theta} = a_3 \dot{\varphi} \dot{\psi} + a_4 \overline{\Omega_r} \dot{\varphi} + b_2 U_3 \\ \ddot{\psi} = a_5 \dot{\varphi} \dot{\theta} + b_3 U_4 \end{cases}$$

$$a_1 = \frac{(I_y - I_z)}{I_x}, a_2 = -\frac{J_r}{I_x}, a_3 = \frac{(I_z - I_x)}{I_y}, a_4 = \frac{J_r}{I_y}, a_5 = \frac{(I_x - I_y)}{I_z}$$

$$b_1 = \frac{\sqrt{2}}{2 I_x} l, b_2 = \frac{\sqrt{2}}{2 I_y} l, b_3 = \frac{1}{I_z} \quad (3.26)$$

Where the inputs  $U = [U_1, U_2, U_3, U_4]^T$  are still the same as in equation (2.37).

### III.4.2 Brushless motor block

To get a little closer to reality we have taken into consideration the dynamics of motors, because each motor supports such a rotation speed. This bloc is divided into three sub blocks:

#### Motor Mixer algorithm

This system takes the commands  $U = [U_1, U_2, U_3, U_4]^T$  corrected by PID controllers as inputs and load of the four motors ( $M_1, M_2, M_3, M_4$ ) as outputs.

$$\begin{aligned} M_1 &= U_1 + U_2 - U_3 - U_4 \\ M_2 &= U_1 - U_2 - U_3 + U_4 \\ M_3 &= U_1 - U_2 + U_3 - U_4 \\ M_4 &= U_1 + U_2 + U_3 + U_4 \end{aligned} \quad (3.27)$$

We assume that the roll in pitch angles are always really small, in this way changing the thrust only meaningfully impacts altitude rate.

#### Motor Transfer function

We have seen in the chapter 2, equation (2.53) that the transfer function needs Li-Po cell voltage to be calculated, as well as the battery discharge function is very important in order to estimate the duration of bearing and operating the motors.



Voltage

We present in the next figure (III.11) the battery discharge algorithm:

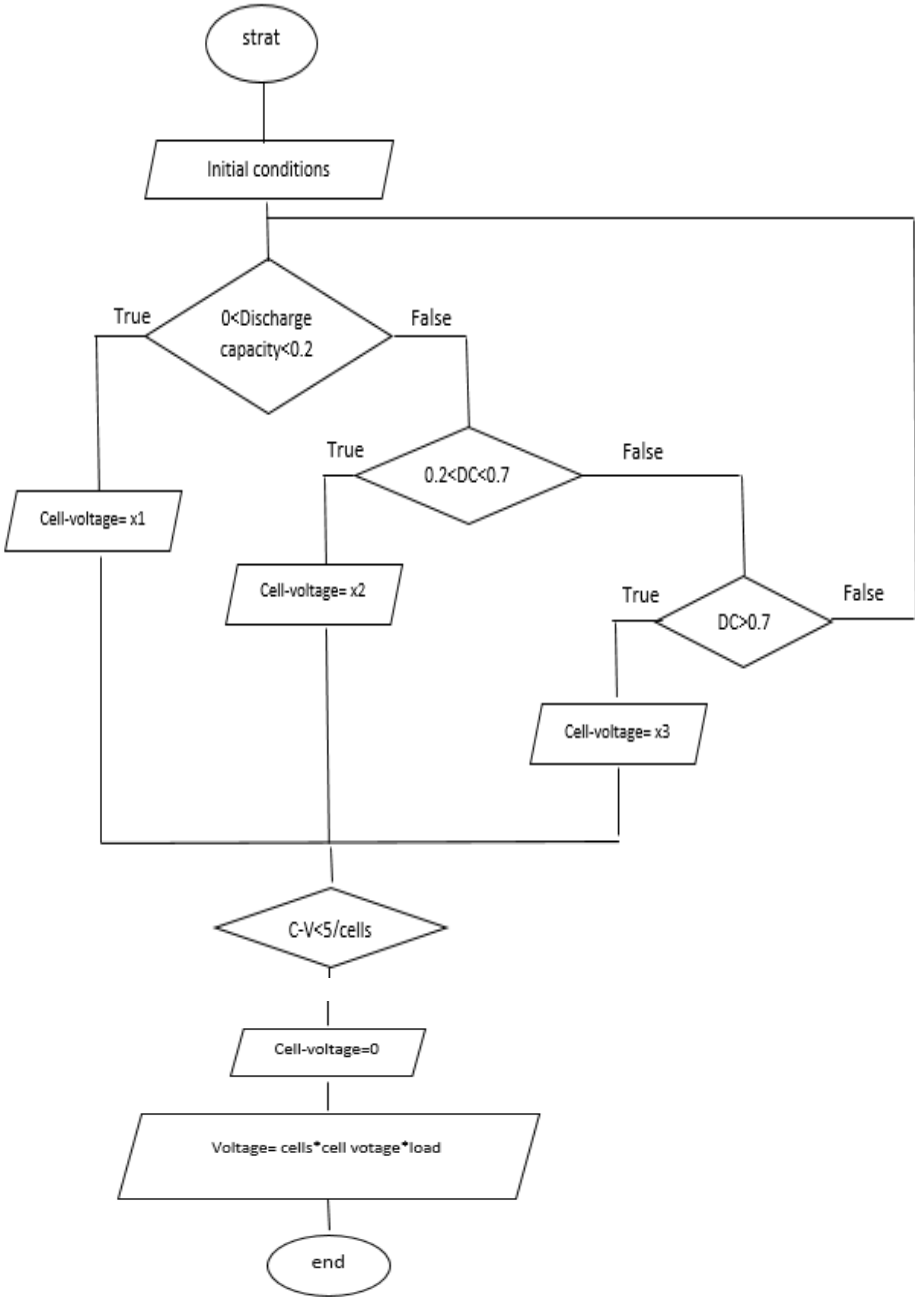


Figure (III -12): Battery discharge algorithm structure

### III.4.3 PID controller block

As we said before, we used The PID technique to control only attitude. The attitude controller takes as an input an error signal  $e$  which is the difference between the desired roll  $\varphi_d$ , pitch  $\theta_d$  and yaw  $\psi_d$  and their actual values  $\varphi$ ,  $\theta$  and  $\psi$ .

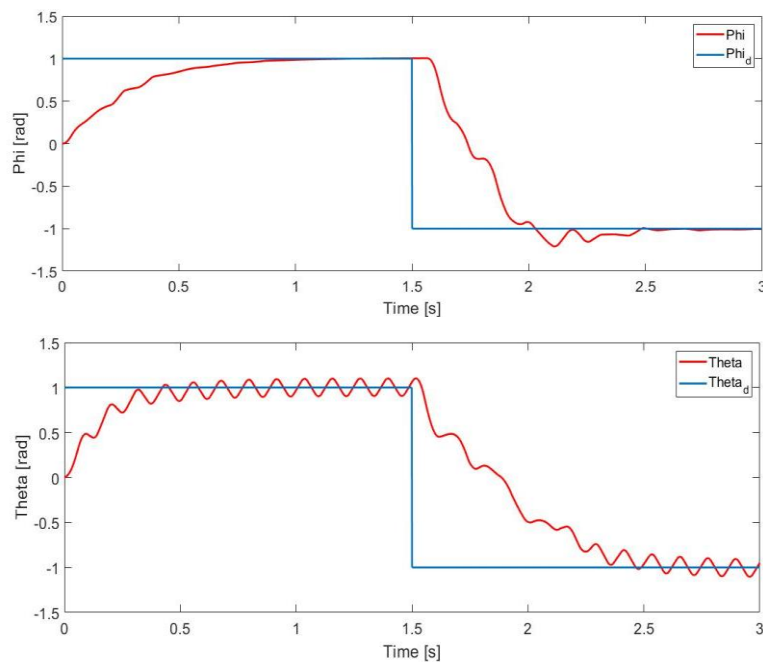
The attitude controller produces the output signals  $U_2$ ,  $U_3$  and  $U_4$  for roll, pitch, and yaw control respectively. So we will need three PID controllers:

$$\begin{cases} U_2 = K_p(\varphi_d - \varphi) + k_d \frac{d(\varphi_d - \varphi)}{dt} + K_i \int (\varphi_d - \varphi) dt \\ U_3 = K_p(\theta_d - \theta) + k_d \frac{d(\theta_d - \theta)}{dt} + K_i \int (\theta_d - \theta) dt \\ U_4 = K_p(\psi_d - \psi) + k_d \frac{d(\psi_d - \psi)}{dt} + K_i \int (\psi_d - \psi) dt \end{cases} \quad (3.28)$$

### III.5 Simulation

To optimize the three control parameters, we ran multiple simulations on Simulink utilizing the entire model. The controller's purpose is to keep the orientation angles stable. The dynamic model in equation (3.25) was utilized for these simulations. In terms of the basic control synthesis technique, the simulated performance was adequate.

The simulation was done giving the results illustrated in Figure (III.12)



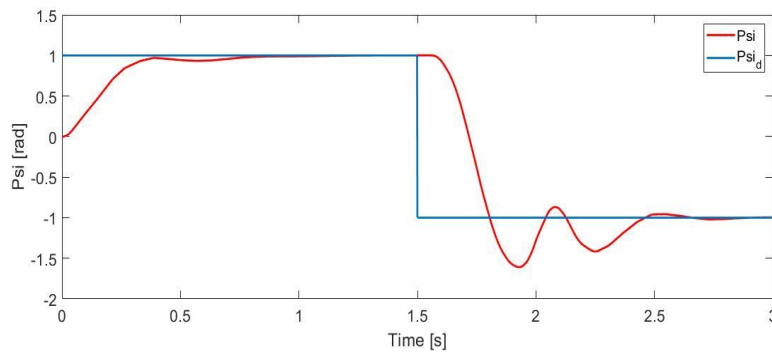


**Figure (III -13):** The measured attitude compared to attitude desired ( $K_p=3$ ,  $k_d=0.8$ ,  $k_i=0.08$  for Roll and Pitch.  $K_p=2.8$ ,  $k_d=0.4$ ,  $k_i=0.03$  for Yaw angle)

Finally, in the next figure we implemented desired angles roll =1, pitch=1, yaw=1.

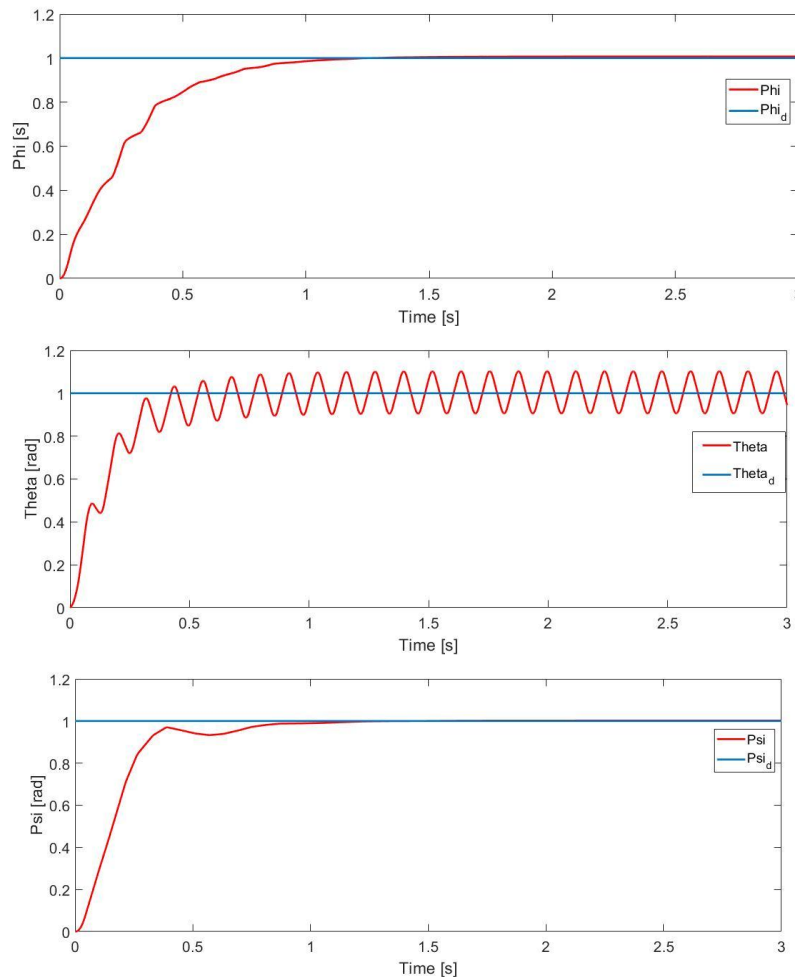


**Figure (III -14):** Simulation results with desired angles roll =1, pitch=1, yaw=1.

Despite changes in consigs that may be regarded as disturbances, the measured values follow the desired values. The results obtained are satisfactory and demonstrate the correct

selection of PID parameters as well as the effectiveness of this regulator in ensuring stability and eliminating statistical error.

### **III.6 Conclusion**

In the first part of this chapter, we identified the parameters in order to populate the mathematical model of our drone, then we generated PID regulators for attitude control, and finally we provided a simulation model to achieve a behavior as close as possible to reality.

We conclude that:

The PID controller is well adapted to the quadrotor when flying near hover and in the absence of large disturbances such as wind.

The PID control law is not a function of the system parameters, but only of the state error, this makes the control law easier to implement and less vulnerable to small variations in system parameters.

In the following chapter, we'll build our quadrotor and go over the various stages of construction and realization.

# **Chapter IV:**

# **Hardware**

# **Implementation**

## IV.1 Introduction

Despite the fact that a theoretical study on several aspects of a quadrotor drone is being conducted, the goal of the project is to implement it in practice by focusing on the most attainable elements, whether on a hardware or software level. As a result, this chapter will cover the wiring of components and different steps we went through during the realization.

We chose to build a drone piloted by ARDUINO for its simplicity and cheap cost.

## IV.2 System architecture

The developed system can be divided into three essential parts. The 1st part is devoted to state estimation through attitude, altitude and position sensors. The 2nd part is dedicated for the transmission of the PID gains in the form of signals. The last part is responsible of the interpretation of the data received from the 1st and the 2nd part, additionally, a PWM measurement is added to system to record the motors inputs. The hardware setup is shown in Figure (IV.1):

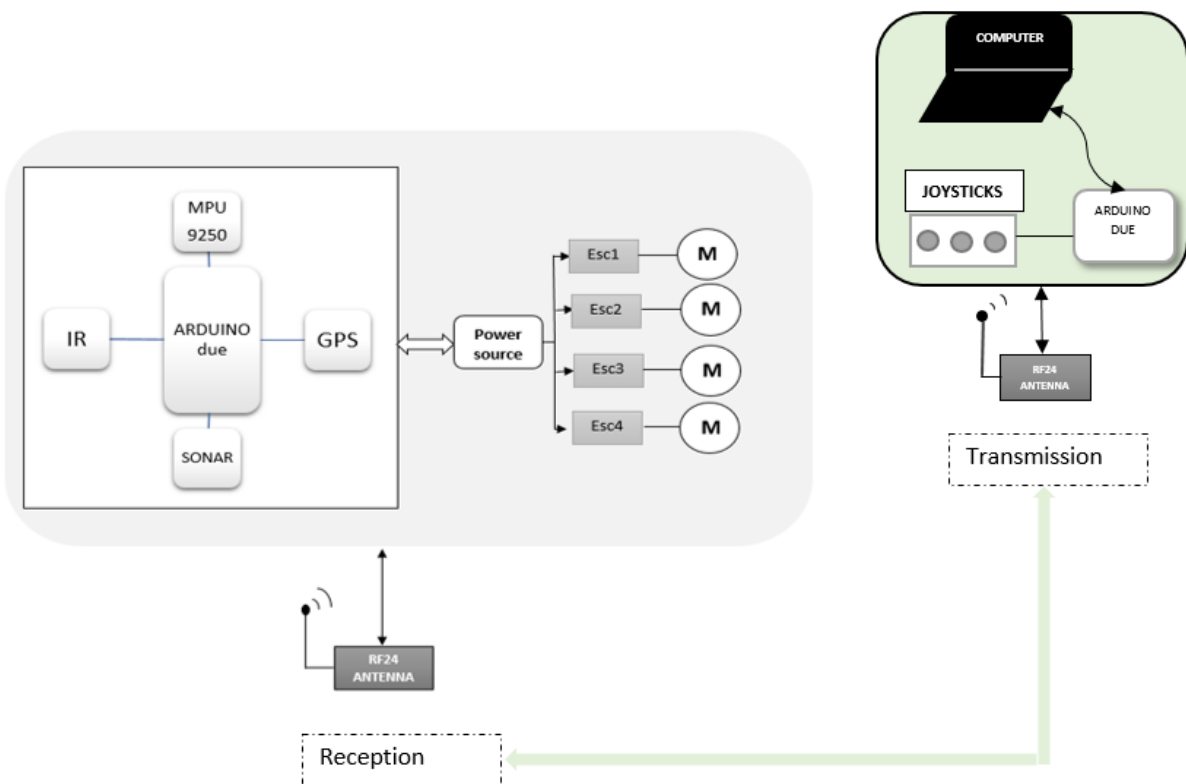


**Figure (IV-1):** Realization architecture

## IV.2.1 Sensors

A drone needs sensors to stabilize and move. We used four sensors:

### Inertial Measurement Unit MPU 9250

The MPU-9250 is a 9-axis Motion Tracking device that combines a 3-axis gyroscope, 3-axis accelerometer, 3-axis magnetometer, and a digital motion processor into one device. This module has three 16-bit ADCs for digitizing the gyroscope outputs and three 16-bit ADCs for digitizing the accelerometer outputs. It is based on the IC MPU-9250, which is the world's smallest 9-axis Motion Tracking device and integrates the latest InvenSense design advancements [24].

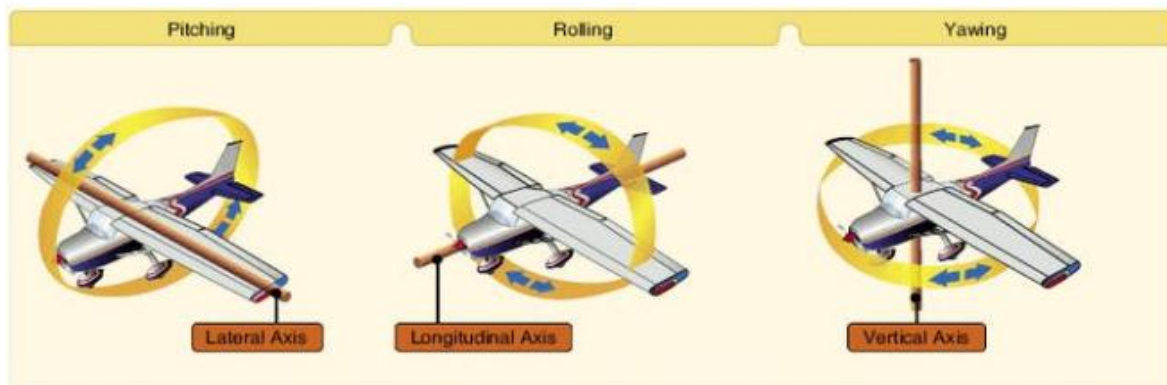


**Figure (IV -2): MPU 9250 motions along the three axis**

The characteristics are presented in the table below:

**Table (IV -1): MPU 9250 specifications**

Input voltage	3 to 5 V
Gyroscope measurement range	$\pm 250, 500, 1000, 2000^\circ / s$
Accelerometer measuring range	$\pm 2, 4, 8, 16 g$
Magnetometer measuring range	$\pm 4800 \mu T$
Interface	I2C, SPI
Resolution	16 bit

Our MPU9250 uses I2C bus Multi master Multi slave. I2C is a simple two-wire serial protocol used to communicate between two devices in an embedded system. It has two lines: SCL used for clock and SDA used for data.

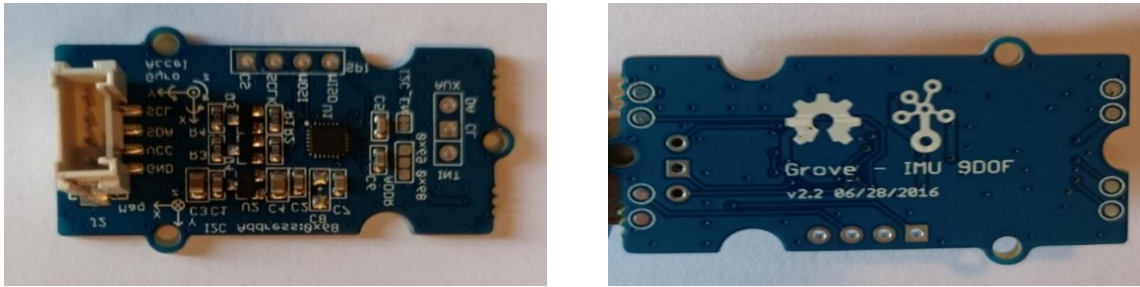


**Figure (IV -3):** MPU 9250 sensor

**SONAR module**

The word SONAR stands for Sound Navigation And Ranging, and it refers to a sensor that uses ultrasound waves to measure distance. According on the required features, there are many different types of SONAR systems [14].

In this work the model HC-SR04 has been adopted. This ultrasonic distance sensor allows distance measurements ranging from 2cm to 450cm with an accuracy of up to 3mm. The angle of the measuring cone is approximately 15 °. The HC-SR04 sonar consists of an ultrasound transmitter, an ultrasound receiver and a control circuit.

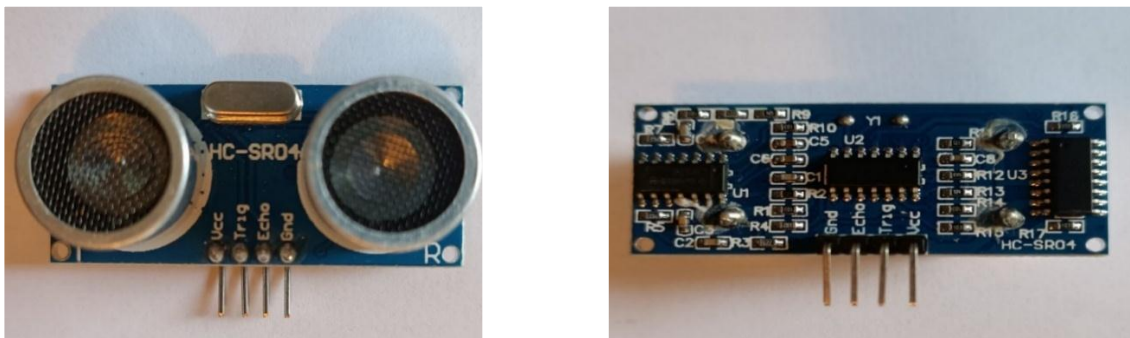


**Figure (IV -4):** HC-S04 SONAR sensor

**Infra-Red module**

IR is the acronym of Infra-Red, which identifies a light wave within a certain frequency range. These waves can't be seen by humans because human eyes are not sensible in this interval (even though IR is quite close to the visible range) [14].

The IR module is a sensor that uses infrared radiation to measure distance. There are a lot of different types of these systems according to the desired characteristics and the technology used for the ranging (triangulation, phase shift, time of flight).



## Chapter IV:

## Hardware Implementation

In this work the model MH-sensor series Flying Fish has been adopted. It is composed of one light emitter, one light detector, a signal processing circuit and other needed circuitry.

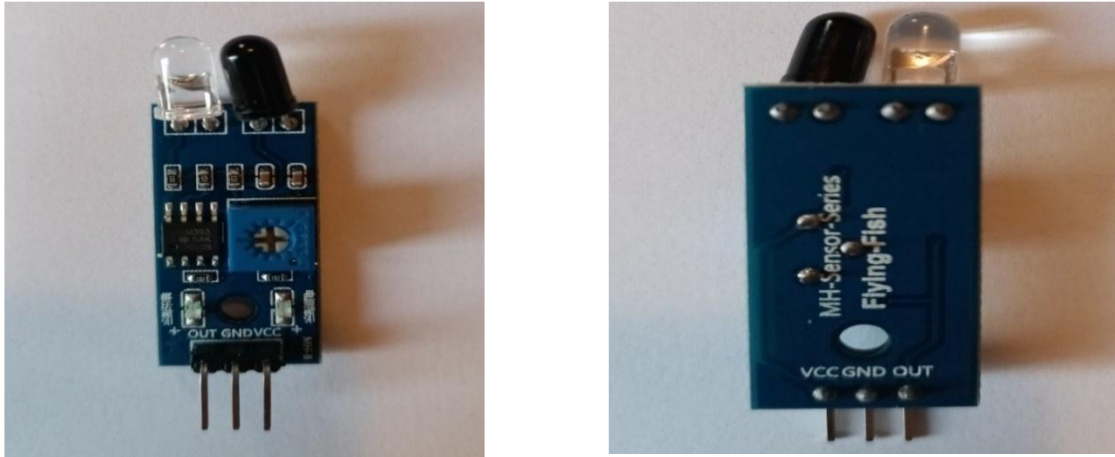


**Figure (IV -5):** *Infra-Red Sensor*

The transmitting tube sends a certain IR frequency which will be reflected when detecting obstacles (reflective surface) and received by the reception of the tube. After processing with the comparator circuit, the green light is on, and the signal output interface outputs a digital signal (low voltage signal).

The MH-sensor series Flying fish has the following specifications:

**Table (IV -2):** *InfraRed specifications*

Operating voltage	3.3 ~ 5V
Detection range	2 ~ 30cm
Detection angle	35 °
Wiring	VCC-VCC; GND-GND; OUT-IO
Dimensions	4 x 1.5 cm
Weight	about 3g

Table IV.2: InfraRed specifications

### GPS Module

The GPS module allows the drone to know its position relative to a network of orbiting satellites. Connecting to signals from these satellites allows the drone to perform functions such as position hold autonomous flight and waypoint navigation. We have used GPS neo-7-m-0-000 with the following specifications:

**Table (IV -3):** *GPS neo-7m-0-000 technical specifications*

Alimentation	Via micro USB / 3.3 or 5v Vcc via VIN
Interface	UART via TX and RX pins
Bit rate	9600 Bps
Antenna	Integrated and external with SMA connector
Dimensions	40 x 25 x 15 mm
Weight	15 gr



**Figure (IV-6):** *GPS neo-7m module*

**Remark:** we have used an indicator LED connected to PIN 13, which lights up during transmission or reception.

**IV.2.2 Emission part**

It is a communication module whose purpose is to be able to communicate with the drone. Either to send him instructions or to receive information. The circuit includes an ARDUINO due board, two or three potentiometers (as needed), Radio transceiver RF24L01. Whereas the wiring must be same as in the following table:

**Table (IV-4):** *The pinout specifications of the emission circuit*

1 <sup>st</sup> Potentiometer (PID gains)	Arduino Due
VCC	5V
GND	GND
SIGNAL	A0
2 <sup>nd</sup> potentiometer (PID gains)	Arduino Due
SIGNAL	5V
GND	GND
SIGNAL	A1
3 <sup>rd</sup> potentiometer (throttle)	Arduino Due
VCC	5V
GND	GND

SIGNAL	A2
RF24L01 module	Arduino Due
VCC	3.3V
GND	GND
CSN	Pin9
CE	Pin8
SCK	SCK (SPI)
MOSI	MOSI (SPI)
MISO	MISO (SPI)
IRQ	Not connected

Table IV.4 : The pinout specifications of the emission circuit

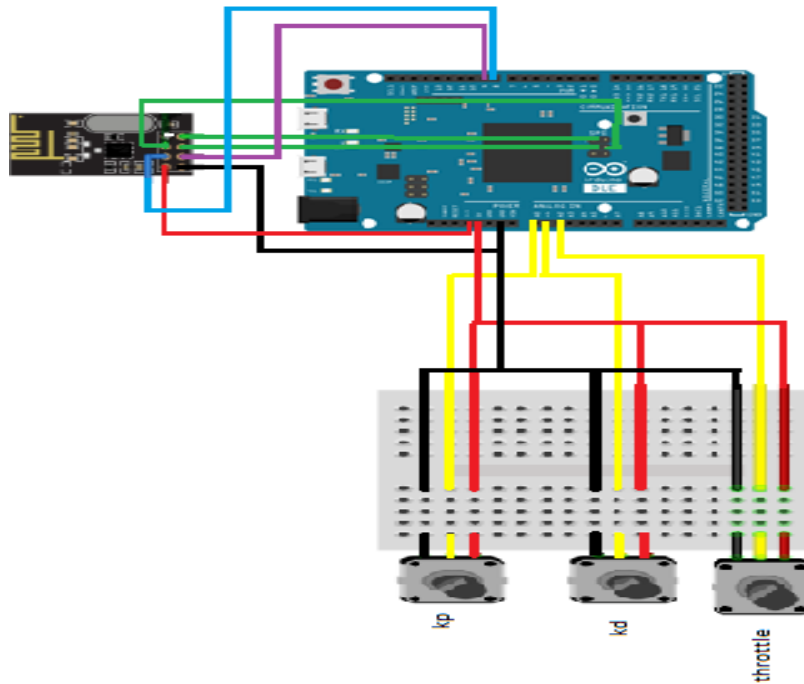
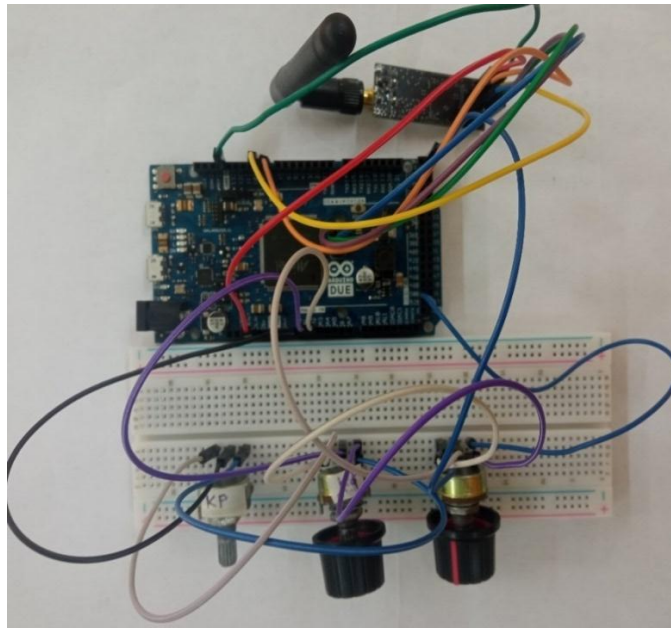


Figure (IV -7): Emission circuit



**Figure (IV -8):** *Assembly of the transmission circuit*

In our project we encountered multiple problems such as interception, signal cut off and external interference. To solve these problems, we reduced the Power Consumption of the nRF24L01 Transceiver by adding a capacitor.

### **IV.2.3 Reception part**

The system is governed by the main microcontroller board which is sufficiently powerful for normal control processing tasks. This embedded card Arduino Due has enough communication ports to drive the other attached boards.

The inertial navigation system (INS) is the detection of our avionic system. It consists of an inertial measurement unit (IMU), global positioning system (GPS), Infra-Red and ultrasonic sonar.

IMU's code is open source, allowing us to adapt it to meet our own design requirements.

An Infrared and Ultrasonic sonar are added to the INS. The sonar is placed beneath the platform, facing the ground, and analyzes ultrasonic signal reflections to produce precise relative height data.

The platform body structure is robust and lightweight, composed of glass fiber and polyamide nylon. It includes four sets of rotors with high-performance 8-inch propellers and

## Chapter IV:

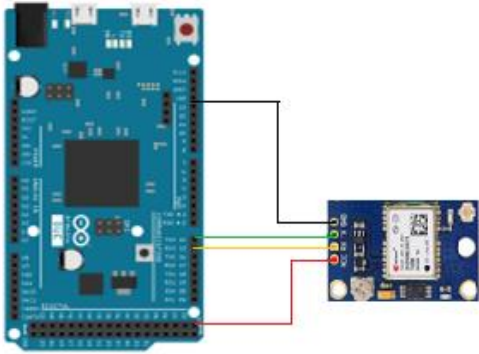
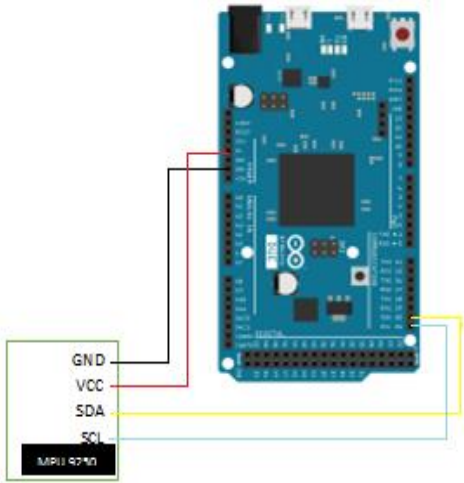
## Hardware Implementation

high-frequency ultra-pulse width modulation (PWM) supported motor drivers and electronic speed controllers.

The battery is positioned under the center of the frame ensuring that the center of gravity (CG) is near the central axis in order to counter the weight produced by adding the onboard system.

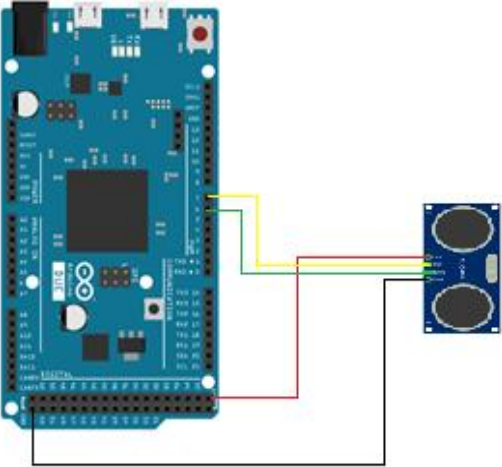
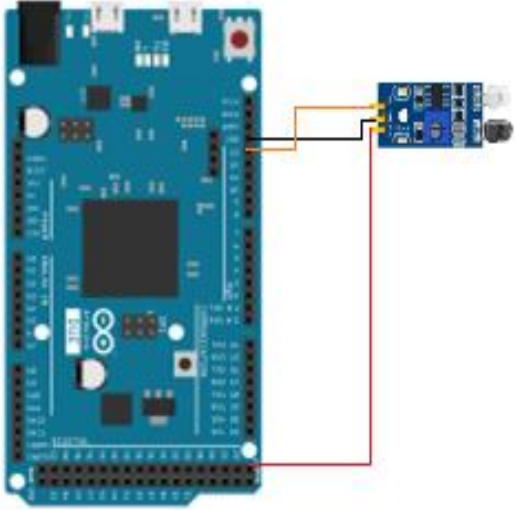
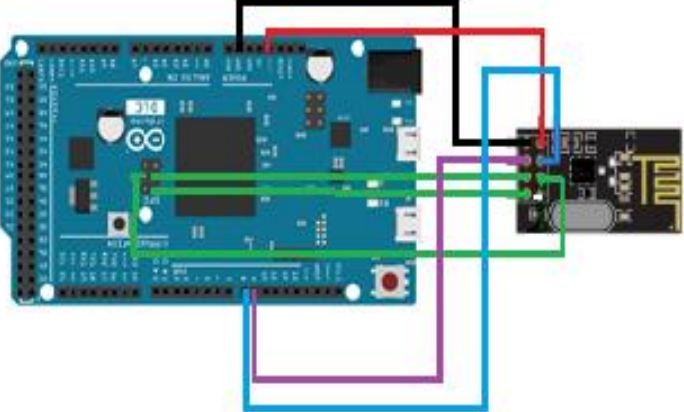
An RF24 module with an antenna was used to enable signal transmission between the two sides of the system. Whereas the wiring must be same as in the following table:

**Table (IV -5):** The pinout specifications of the reception circuit

GPS module	Arduino DUE	Figure (IV -19): GPS module Wiring
Vcc GND TX RX	5V GND TX3 RX3	
MPU9250	Arduino DUE	Figure (IV -20): MPU9250 module wiring
Vcc GND SDA SCL	5v GND SDA20 SCL21	

## Chapter IV:

## Hardware Implementation

<p><b>Sonar</b></p> <p>Vcc GND ECHO TRIG</p>	<p><b>Arduino DUE</b></p> <p>5v GND Pin 6 Pin 7</p>	<p><b>Figure ( IV -21):</b> Sonar Module Wiring.</p> 
<p><b>IR module</b></p> <p>Vcc GND Digital Output</p>	<p><b>Arduino DUE</b></p> <p>5v GND Pin 13</p>	<p><b>Figure (IV -22):</b> IR module wiring</p> 
<p><b>RF24L01</b></p> <p>Vcc GND CSN CE SCK MOSI MISO IRQ</p>	<p><b>Arduino DUE</b></p> <p>3.3 V GND pin 9 pin8 SCK (SPI) MOSI (SPI) MISO (SPI) Not connected</p>	<p><b>Figure (IV-23):</b> RF24 module Wiring</p> 

The general circuit of our project is represented in the next figure (IV.14):

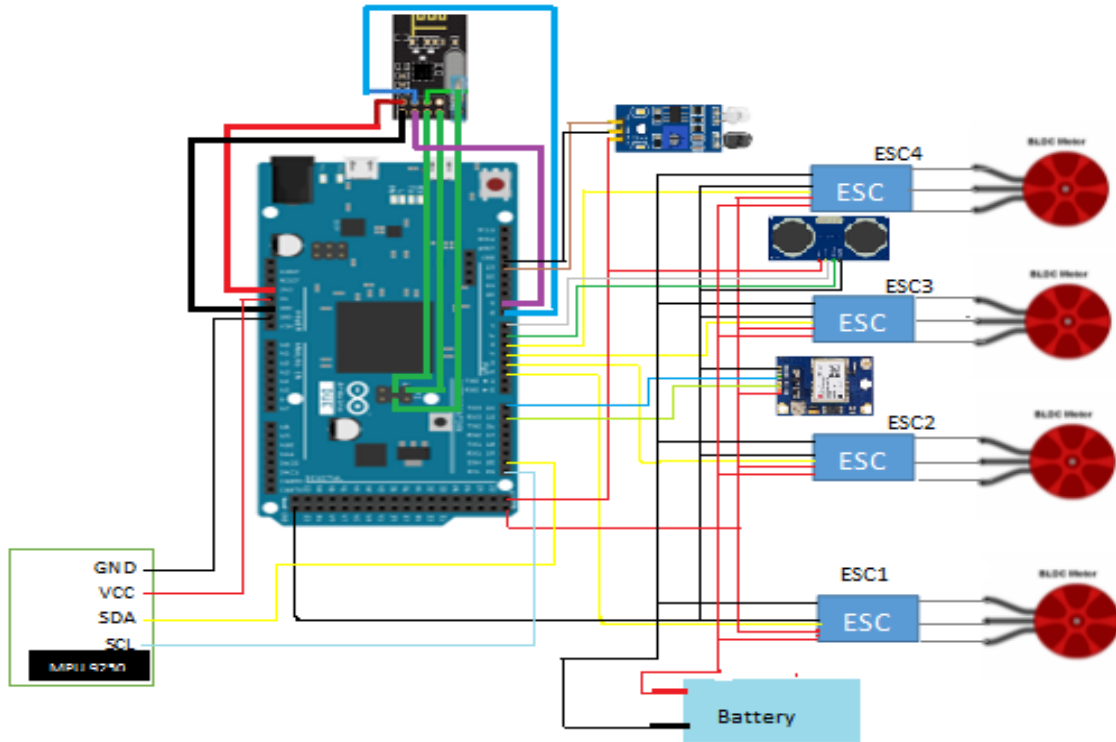


Figure (IV -14): The general circuit of the quadrotor

### IV.3 Quadrotor Assembly

The motors are attached to the ends of the frame, the ARDUINO board in the center, and the distributor below as the following figure shows:



Figure (IV -15): Quadrotor assembly



Now as you can see to eliminate the maximum number of wires we have produced an electronic PCB.

### Conception of the printed circuit board

The PCB ("Printed Circuit Board") refers to the printed circuit of an electronic device, which is also sometimes called "electronic card". This circuit is made of an insulating material on which thin layers of copper are etched on a set of tracks, terminated by holes in which electronic components are implanted. The final result looks as follows :



**Figure (IV -16):** *Quadrotor and PCB assembly.*

## IV.4 Calibrations

### ESC Calibration

Most ESC's need to be calibrated so that they know the minimum and maximum PWM values that the flight controller will send. There are several calibration methods, in our case we followed these steps:

- a) Without powering the ESC's. Set the potentiometer to full (2000us).
- b) Connect the battery.
- c) After several beeps are emitted corresponding to the number of cells of the battery (in our case 4 beeps because it is a 4S LIPO), place the potentiometer in the lowest position (1000us).



- d) A long beep is emitted signifying that the "engine stop" position has been recorded by the ESCs.
- e) Disconnect the battery.

### IMU Calibration

The purpose of the calibration is to give a reference point to the sensor and the point that will be given to it corresponds to an inclination of 0 degrees.

Our IMU must be placed at the center of gravity of the drone for good results, away from ESCs and motors to eliminate maximum vibrations where the calibration is done using an ARDUINO program:

- a) read the sensor.
- b) Calculate offsets of gyroscope, accelerometer and magnetometer.
- c) Write down offsets so you can set them in your projects.
- d) Verify that the calibration worked by measuring the angles and compare them with the Quadrotor inclination.

### IV.5 Test Bench

Test bench aims, to fill the gap between simulation and real time flight. First, to simplify the task we used the following test bench which performs the control along one axis (either roll or pitch), and observe its behavior.

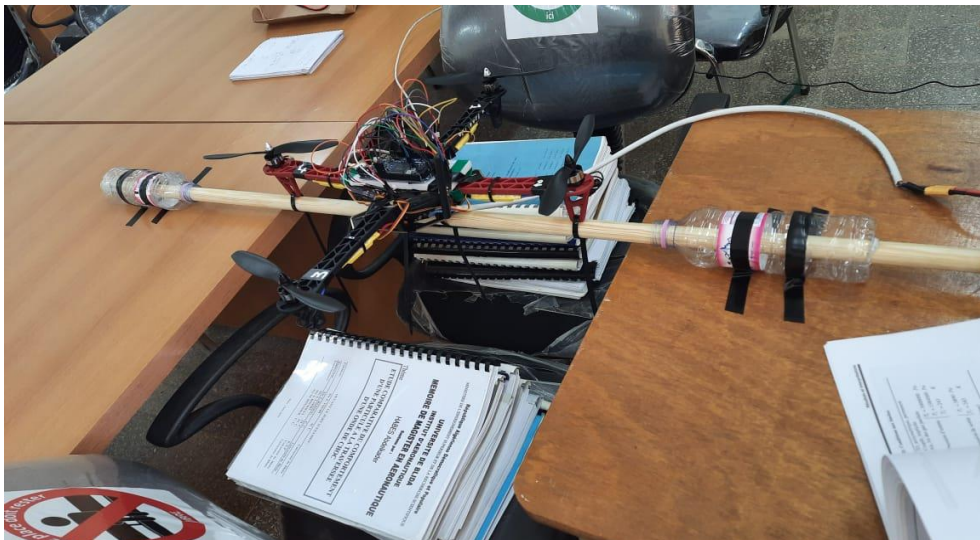


**Figure (IV -17):** *Single axis test bench*

## Chapter IV:

## Hardware Implementation

After that, we built a second test bench presented below. The test bench was built in such a way that allows the quadrotor to change its orientation in three degrees of freedom but keeping its position fixed, that's why we attached three frames and a stick where the drone must be attached in its center of gravity.



**Figure (IV -18):** *Back view of the three frames test bench.*

Finally, to eliminate all frictions and for more flexibility a third test bench was used.

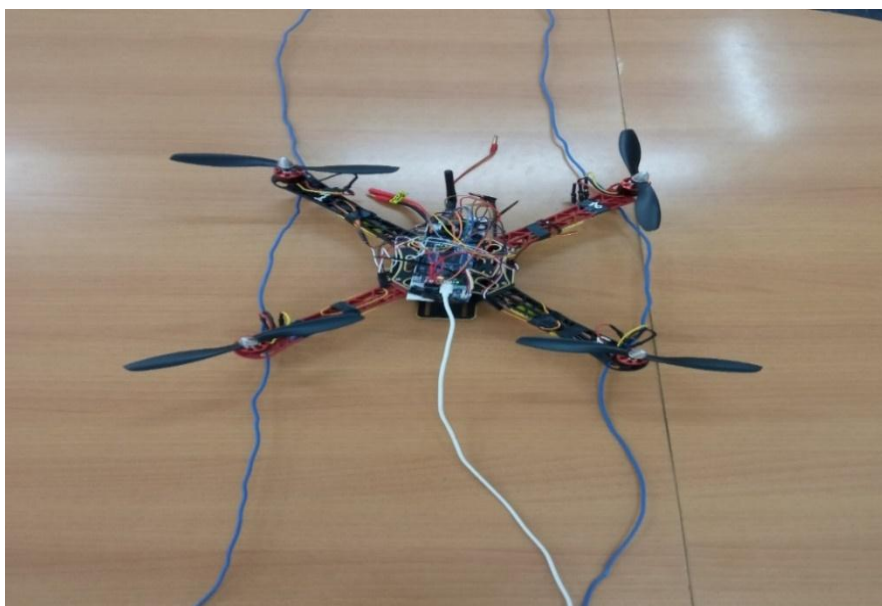


**Figure (IV -19):** *Two wires test bench*

**IV.6 PID Tuning and Regulation**

In this project we used the MPU9250 sensor which is able to calculate the angles of rotation along the three axes x, y, z. These angles are roll, pitch and yaw respectively ( $\varphi$ ,  $\theta$ ,  $\psi$ ). So we used 3 PID regulators for the inner loop, and to determine the values of the coefficients  $K_p$ ,  $K_i$ ,  $K_d$  for the three PID controllers, we used the Tuning method. As the motors are organized in a square, the coefficients of the pitch & roll angles are the same. Which makes 6 values in total to define. We have followed these steps:

- First started by ROLL control.
- Initialize all the coefficients to zero.
- So that the system reacts quickly we increase the value of  $K_p$  until the Quadrotor starts to oscillate.
- Decrease this value by 25% to fall into the value that suits us best.
- To reduce these oscillations and gain stability, the value of  $K_d$  is gradually increased.
- Finally to improve the precision of the system, we increase the value of  $K_i$  in steps of 0.01.

We will follow the same method for the 3 movements to obtain at the end the following values:

**Table (IV -6): PID gains representation**

PID Coeff	Roll	Pitch	Yaw
$K_p$	2.98	2.98	2.8
$K_d$	0.6	0.6	0.4
$K_i$	0.06	0.06	0.03

**IV.7 Conclusion**

The creation of an aerial vehicle controller is often a lengthy and risky process. It requires a series of tests, ranging from simulation to real-world flying. However, due to the limitations of the present simulation approach, there are discrepancies between simulation and real-time flight.

Despite the simplicity of the techniques and materials, that we used to complete this project especially the ARDUINO board which is known by its long response but we managed to stabilize the two movements (roll and pitch); thanks to a robust control law (PID) and the IMU board.

### General Conclusion

There are many types of UAV's in terms of their shape, function, size, etc. In our project, we have switched to quadrotors due to their mechanical simplicity and ease of control thanks to the PID controllers.

Our project is divided into several sections, we started with a theoretical study including simulation and then think about how to make an autonomous mini drone and the elements common to this application such as the Arduino and speed controllers followed by the study of air navigation detectors and their choice, the next step was to conduct flight tests, in which we utilized three test benches, one of which is distinguishable from the others in a feature, and compare theoretical results with field measurements to see if any improvements could be made.

The goal of all this, is to find the appropriate and ideal PID gains for our plane, fortunately we were able to stabilize the quadrotor in the two axis roll and pitch. We conclude that:

- Quadrotor is an under actuated system.
- New technologies such MPU-9250, GPS-7m neo, Arduino Due allowed to reduce costs and simplify the implementation.
- Quadrotor is very sensitive vehicle where interference between the cables could lead to damage it, or a little gust of wind could destabilize it but fortunately scientists have developed other control laws and algorithms such as back-stepping, fuzzy logic, etc.
- The cross style quadrotor could provide high maneuverability as compared to standard quadrotors.
- In the X configuration for all degrees of motion, all the rotors are participating to perform the desire displacement, which is the main advantages of cross structure.
- A last improvement is done by replacing the remote controller with a PC to be able to provide more complex tasks.
- Although the simulator showed not really good accuracy results, but it is helpful to simulate the environment as well and use tools that interact with the real platform.

## **General conclusion**

Our project is open to several perspectives and applications. By modifying or adding a few things in hardware or software will be able to completely change the function / mission of the drone, for example, the camera can be used to measure and correct the position or speed, detecting obstacles, tracking objects, etc. The future of drones is limitless.

## Simulation

The Simulink model of the quadrotor is as follows:

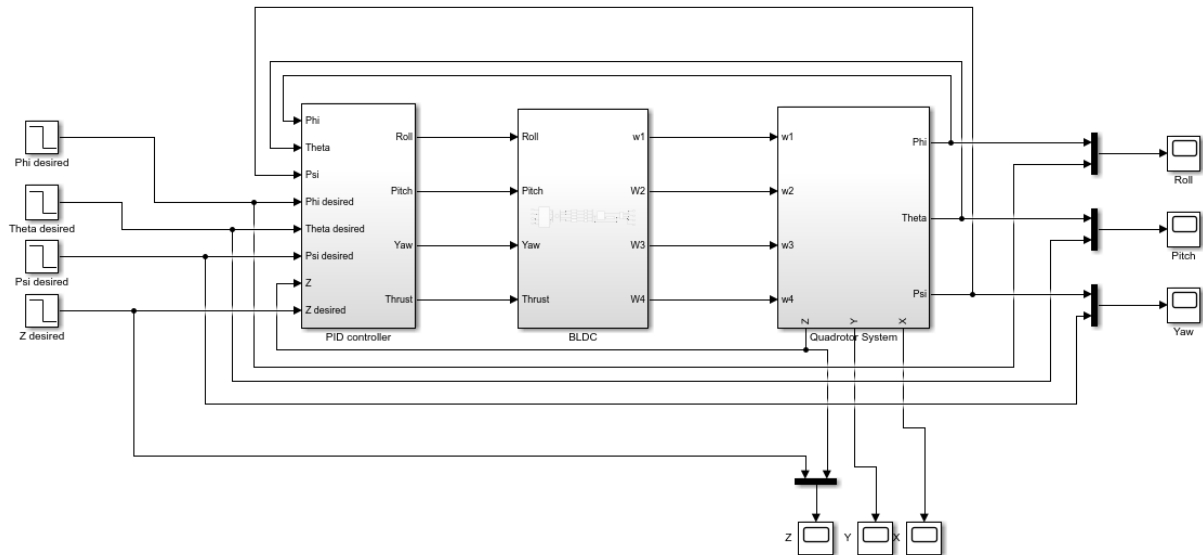
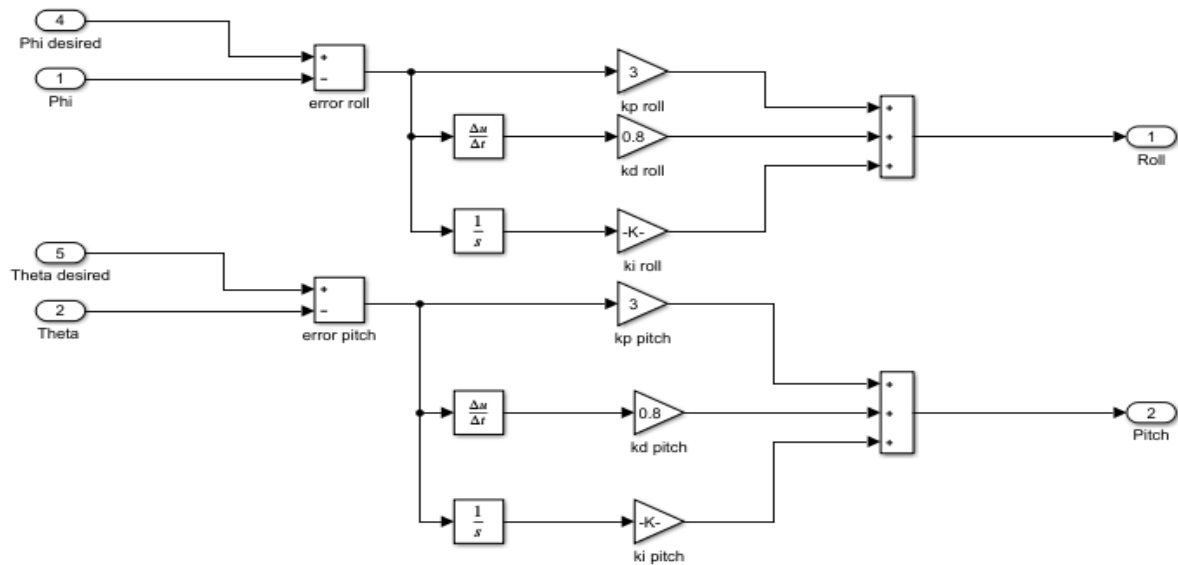


Figure A.1: Simulink model of the quadrotor.

The figure (A.2) shows the inside of the “PID controller” block:



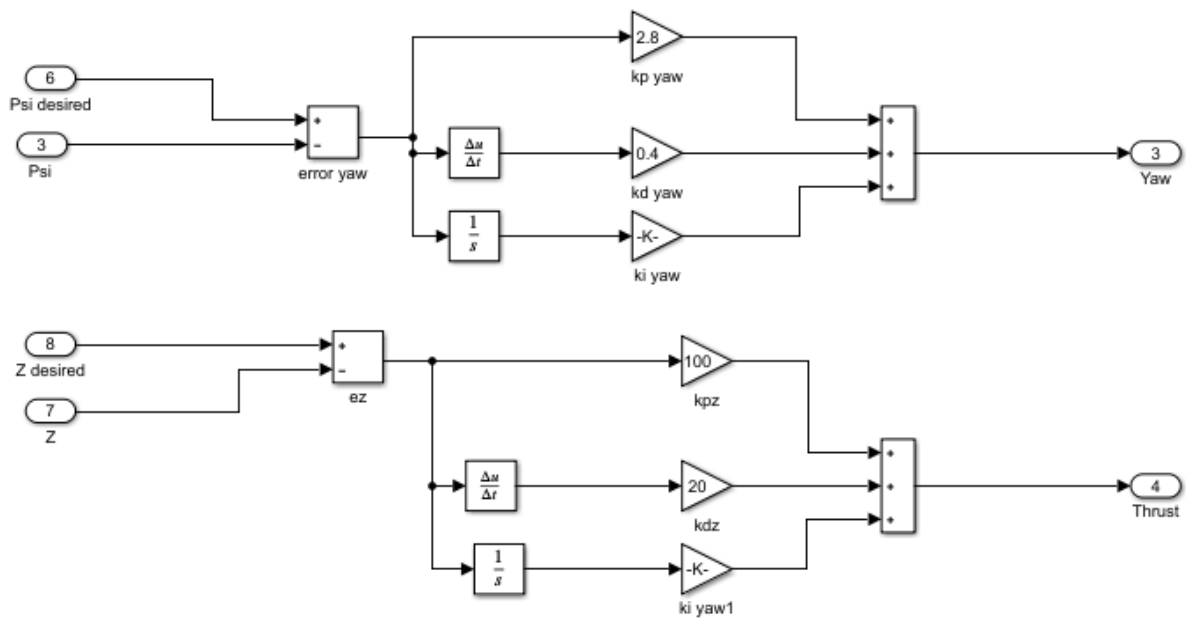


Figure A.2: PID controller Simulink Block.

The following figure shows the dynamics of motors:

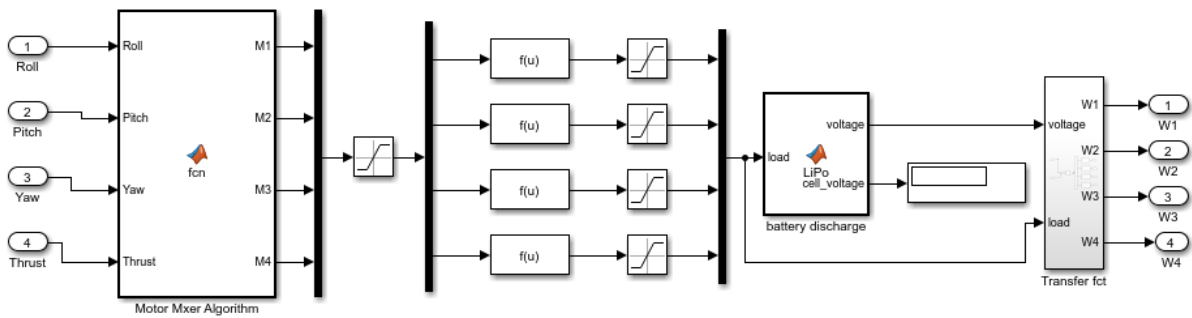


Figure A.3: Brushless motor Simulink block.

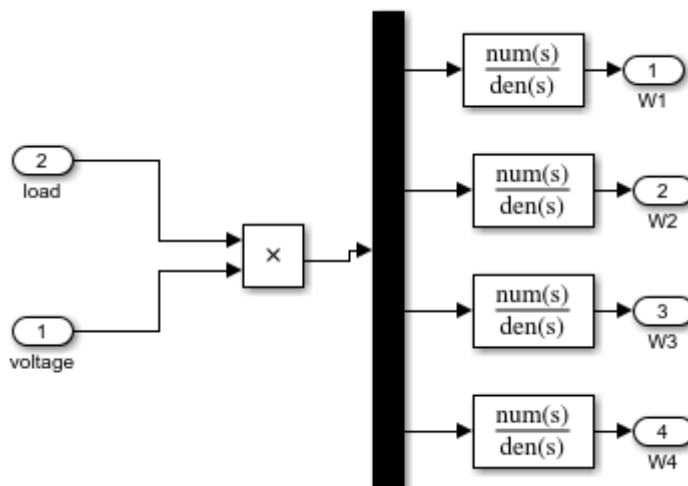


Figure A.4: TF BLDC

The last block “Quadrotor model” is dedicated to the modeling of our drone including angles and position.

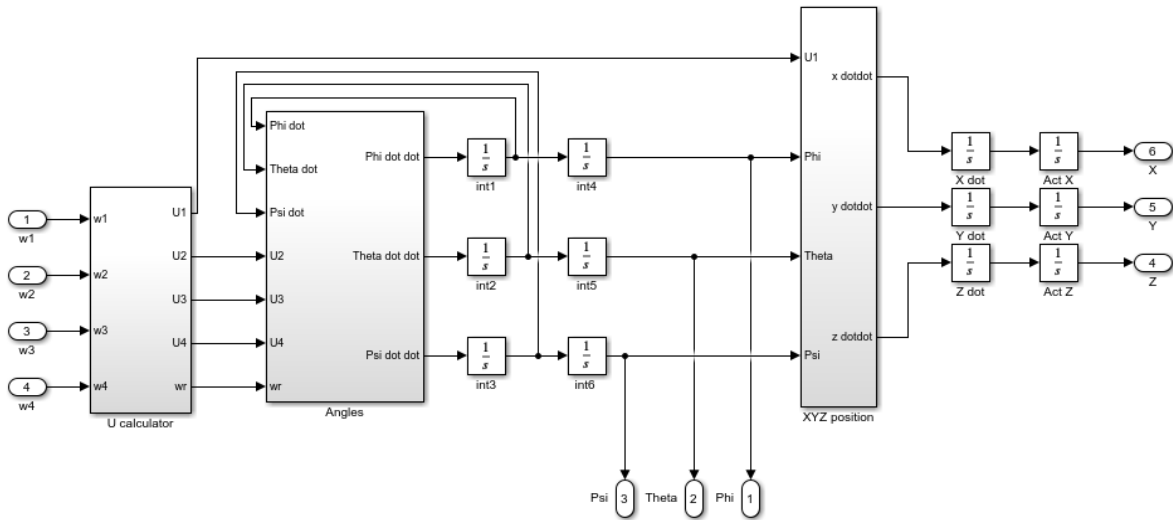


Figure A.5: Quadrotor model Simulink block.

The following figures show the Ucalculator,Angles and XYZ Position blocks respectively:

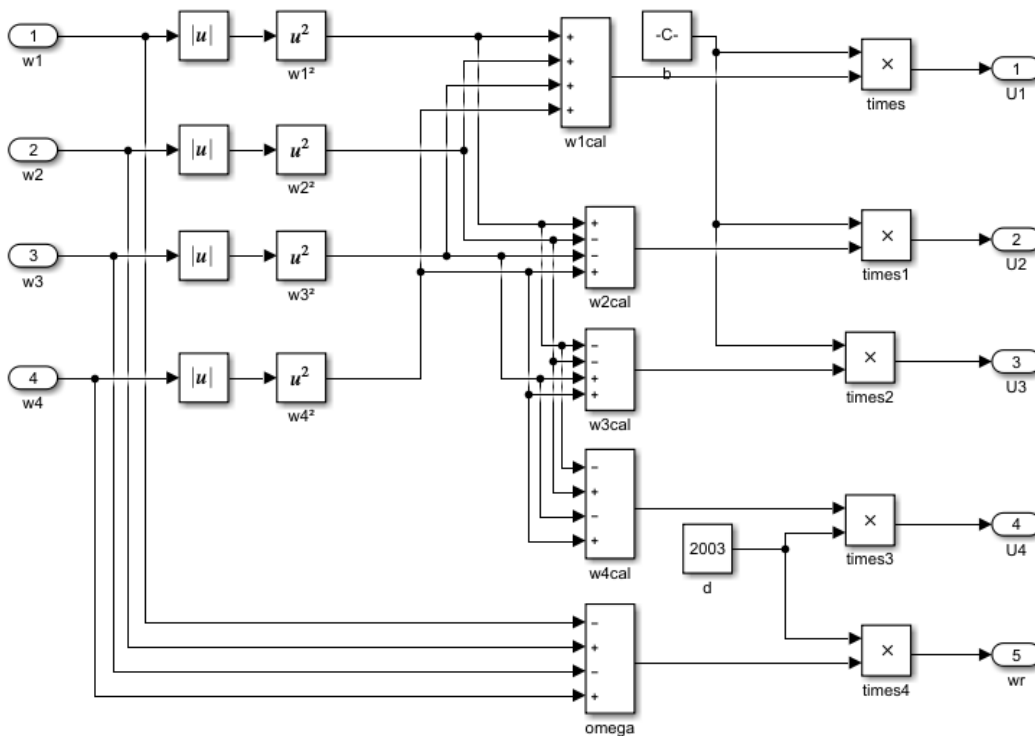


Figure A.6: U calculator.



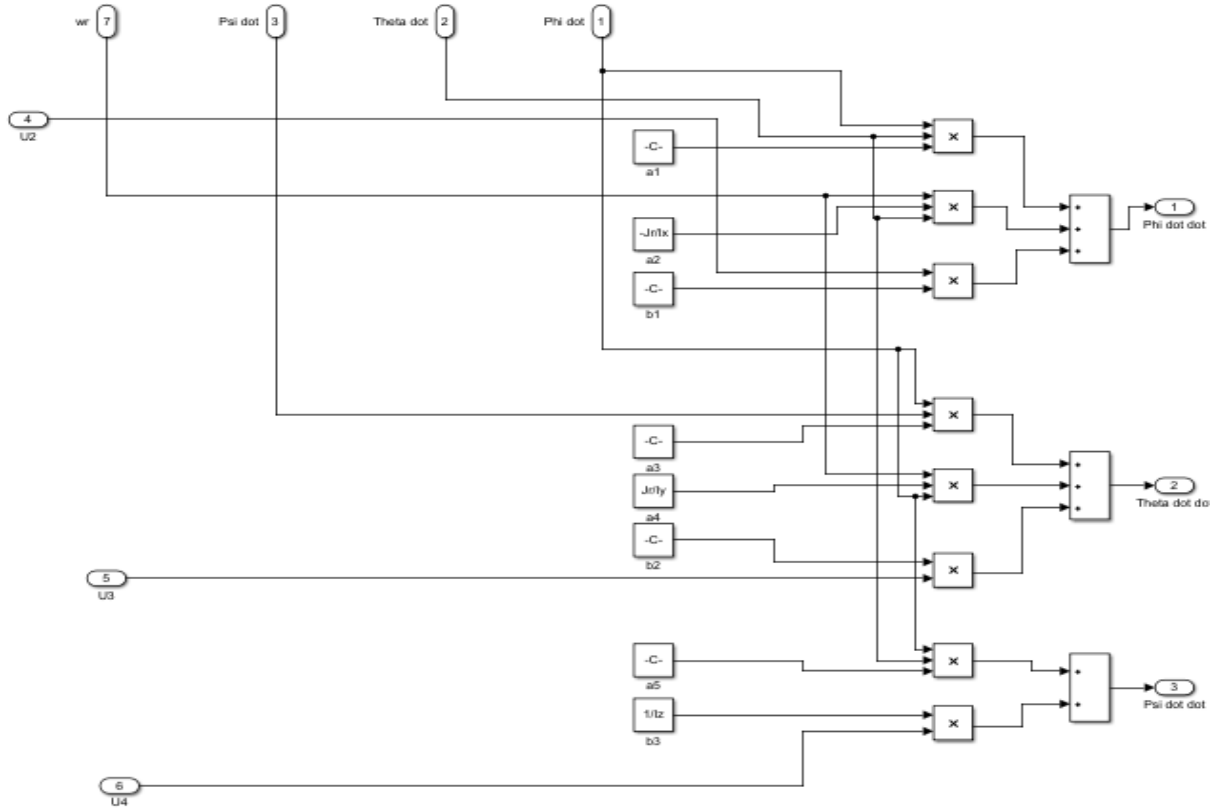


Figure A.7: Angles.

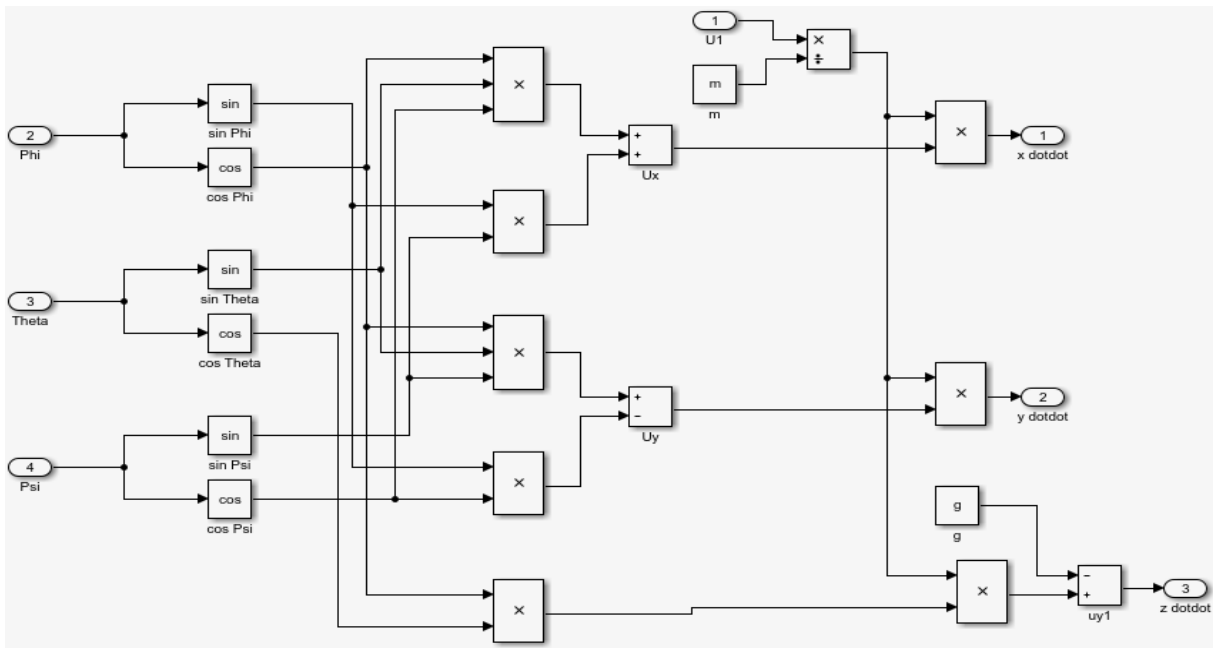


Figure A.8: XYZ Position

## Appendix

And finally, a feedback is provided to compare between the desired state and the estimated state.

For the first experience we have entered the PID gains found in the realization after that PID tuning was done to choose adaptive gains.

## Bibliography

- [1] ElKholy, H. M. (2014). Dynamic modeling and control of a quadrotor using linear and nonlinear approaches. American University in Cairo.
- [2] [website] <https://doctorpreneurs.com/9-drones-that-will-revolutionise-healthcare/>
- [3] Romero, L. E., Pozo, D. F., & Rosales, J. A. (2014). Quadcopter stabilization by using PID controllers. *Maskana*, 5, 175-186.
- [4] [website] <https://store.arduino.cc/arduino-due>
- [5] [website] <http://caetesnews.com.br/metallic-forest/dc-motor-in-proteus.php>
- [6] [website] <https://howtomechatronics.com/how-it-works/how-brushless-motor-and-esc-work/>
- [7] [website] <https://www.techopedia.com/definition/8093/lithium-polymer-battery-lipo-battery>
- [8] [website] <https://culturefpv.fr/comprendre-les-lipo-20171007/>
- [9] nRF24L01 Single Chip 2.4 GHz Radio Transceiver, March 2006, Nordic Semiconductor ASA – World Wide Distributors, Vestre Rosten 81, N-7075 Tiller, Norway
- [10] Khebbache, H. (2012). Tolérance aux défauts via la méthode backstepping des systèmes non linéaires Application: Système UAV de type Quadrirotor (Doctoral dissertation, Université de Sétif 1-Ferhat Abbas).
- [11] [website] <https://www.monolithicpower.com/en/brushless-vs-brushed-dc-motors>
- [12] Oguntoyinbo, O. (2009). PID control of brushless DC motor and robot trajectory planning simulation with MATLAB®/SIMULINK®.
- [13] Mustapa, Z., Saat, S., Darsono, A. M., & Yusof, H. H. (2016). Experimental validation of an Altitude control for quadcopter. *ARPN J. Eng. Appl. Sci.*, 11(6), 3789-3795.
- [14] Bresciani, T. (2008). Modelling, identification and control of a quadrotor helicopter. MSc theses.
- [15] McKerrow, P. (2004, April). Modelling the Draganflyer four-rotor helicopter. In *IEEE International Conference on Robotics and Automation, 2004. Proceedings. ICRA'04. 2004 (Vol. 4, pp. 3596-3601)*. IEEE.
- [16] UAB-Tlemcen, B. C. P. P., & UAB-Tlemcen, E. P. Conception et commande d'un quadrotor UAV à base d'Arduino.
- [17] Ivanov, R. State Estimation Filters. Department of Computer and Information Science, Philadelphia.
- [18] Caruso, M., Sabatini, A. M., Laidig, D., Seel, T., Knaflitz, M., Croce, U. D., & Cereatti, A. (2021). Analysis of the Accuracy of Ten Algorithms for Orientation Estimation Using Inertial

## Bibliography

- and Magnetic Sensing under Optimal Conditions: One Size Does Not Fit All. *Sensors*, 21(7), 2543.
- [19] *International Journal of Computer Electrical Engineering* Design of a Modified Madgwick Filter for Quaternion-Based Orientation Estimation Using AHRS Amjed S. Al-Fahoum\*, Momtaz S. Abadir Manuscript submitted March 26, 2018; accepted April 15, 2018.
- [20] Tanveer, F., Waheed, O. T., & Rehman, A. (2011). Design and development of a sensor fusion based low cost attitude estimator. *J. Sp. Technol.*, 1(1).
- [21] Kuipers, J. B. (1999). *Quaternions and Rotation Sequences: A Primer with Applications to Orbits, Aerospace and Virtual Reality*. Princeton, NJ, USA: Princeton University Press.
- [22] Madgwick, S. O., Harrison, A. J., & Vaidyanathan, R. (2011, June). Estimation of IMU and MARG orientation using a gradient descent algorithm. In 2011 IEEE international conference on rehabilitation robotics (pp. 1-7). IEEE.
- [23] [website] <https://nitinjsanket.github.io/tutorials/attitudeest/madgwick>
- [24] [website] <https://www.elecrow.com/imu-9dof-mpu9250-p-1239.html>
- [25] Bouabdallah, S. (2007). Design and control of quadrotors with application to autonomous flying (No. THESIS). Epfl.
- [26] Choutri, K., Lagha, M., & Dala, L. (2021). A Fully Autonomous Search and Rescue System Using Quadrotor UAV. *International Journal of Computing and Digital Systems*, 10, 2-12.
- [27] Choutri, K., Lagha, M., & Dala, L. (2019). Multi-layered optimal navigation system for quadrotor UAV. *Aircraft Engineering and Aerospace Technology*.